Beam Position Monitors

Peter Forck, Piotr Kowina, Dmitry Liakin
Gesellschaft für Schwerionenforschung GSI, Darmstadt, Germany

Abstract
Beam Position Monitors BPM are the most frequent non-destructive diagnostics used at nearly all Linacs, cyclotrons and synchrotrons. BPMs deliver the center-of-mass of the beam and act as a monitor for the longitudinal bunch shape. The signal generation by the beam's electro-magnetic field is described using the transfer impedance concept. Different realizations of BPMs are discussed with the focus on the capacitive linear-cut, button types and stripline BPMs. Wall current monitor based systems and cavity BPM are briefly mentioned. Examples for the design criteria with respect to position sensitivity and linearity are given. The beam's center is determined on quite different time scales from μs for bunch-by-bunch observation up to s for precise closed orbit determination. The resulting requirements for the analogue and digital electronics are discussed.

1 Basic Properties of BPM installations

Electromagnetic pick-ups serve as a non-destructive diagnostic device used very frequently in nearly any accelerator operating with bunched beam. The idea is to measure the charges induced by the electric field of the beam particles on an insulated metal plate, see Fig. 1. Because the electric field of a bunched beam is time dependent, an alternating current (ac) signal is seen on the plate and the coupling is done using radio frequency (rf) technologies. The application is the determination of the beam position (center-of-mass). For this purpose, four pick-up plates are installed crosswise at the beam pipe wall and the difference signals of opposite plates yield the beam's center-of-mass for both transverse planes, respectively. Based on this application, the installation is called a **B**eam **P**osition **M**onitor **BPM** or Position **P**ick-**U**p **PU**. Even in the case of longitudinal bunch shape observation the abbreviation BPM is frequently used although the name 'electro-magnetic pick-up' would better be suited for this application.

In general, pick-ups couple to the electro-magnetic field as generated by the charged particle beam. For relativistic beam velocities the transverse field components in the laboratory frame (i.e. the frame of all hardware installations) increase compared to the values within beam's rest frame. The Lorentz transformation from the beam's rest frame $E_{\perp,rest}(t')$ at time t' to the laboratory frame $E_{\perp,lab}(t)$ at time t for the field component transverse to the direction of motion is given by

$$E_{\perp,lab}(t) = \gamma \cdot E_{\perp,rest}(t') \tag{1}$$

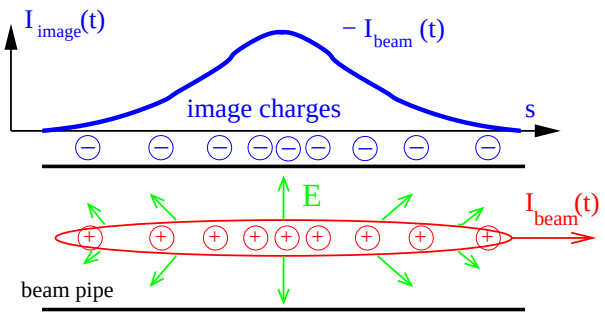

Fig. 1: The beam current induces a wall current of the same magnitude but reversed polarity.

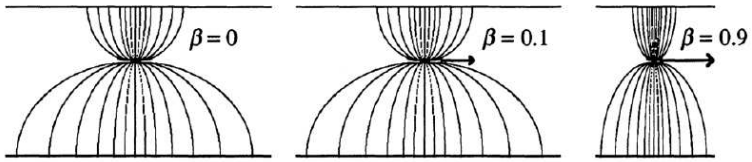

Fig. 2: Schematic plot for the relativistic increase of the transverse electric field.

as schematically shown in Fig. 2. This transverse field component increases with the Lorentz factor $\gamma = 1/\sqrt{1-\beta^2}$ and even for moderate beam velocities the resulting field can be approximated by a so called Transverse Electric and Magnetic field distribution. A TEM mode has the electric and magnetic field vector perpendicular to the propagation direction. For most qualitative considerations and quantitative calculations the beam can be substituted by a TEM wave. One result is that the wall current has the same time behavior as the beam passing by. Only for velocities below about $\beta < 0.5$ major modifications are required. Another valid assumption is that the power coupled out by the detector is much lower than the power carried by the beam; in other words: The beam does not react on the amount of signal strength coupled out. For that reason, the wall current can be modeled as a current source with arbitrary large inner impedance.

The principle signal shape is best described by the so called transfer impedance Z_t, which is basically a frequency dependent quantity transferring the beam current to the usable voltage signal. The properties of this transfer impedance Z_t is described in the second Chapter using a typical installation at a proton and ion synchrotron as an example. The design consideration and realization for proton synchrotrons using the so called **linear-cut BPMs** are discussed in Chapter 3. The advantage of this type is the large signal amplitude and a high linearity with respect to position offsets. But its application is mainly limited to bunches much longer than the BPM length of typically several cm. For shorter bunches, as present at most electron accelerators and proton Linacs, shorter installations are used, the so called **button BPMs**; their properties are discussed in Chapter 4. Linear-cut and button BPMs are treated as devices with capacitive coupling to the beam's electric field, effects related to a signal propagation are not taken into account. This is different to **stripline BPMs** suited for short bunches. Here the signal propagation, in most cases of relativistic beam velocities and corresponding electro-magnetic TEM wave type, has to be included in the design considerations; these BPMs are discussed in Chapter 5. Further BPM principles are mentioned in Chapter 6, which offers either an extended bandwidth for longitudinal bunch structure observations or a higher resolution for the position reading. In particular, the excitation of a resonating mode with a **cavity BPM** offers a higher resolution even for a short beam delivery down to the μs time scale, which is important for modern free-electron lasers or electron-positron colliders.

The signal shape and amplitude is significantly influenced by the processing electronics and therefore the type of electronics is an integral part of the BPM system. In particular, the spatial resolution can widely be varied with the cost of resolution in time. Analog electronic chains are used for this purpose or, for modern installations, the main treatment is done by digital signal processing. Several analog and digital electronic principles are discussed in Chapter 7.

Even though the technical realization of the BPM systems is the main focus of this article, we want to address briefly the most frequent applications based on the determination of the beam center from a bunch-by-bunch time scale up to the position averaged over several seconds:

– For the fast readout, one single value of the horizontal and vertical position is given for each bunch (**bunch-by-bunch** mode). Using this values, one can follow the beam behavior throughout the accelerator and can treat this bunch as a 'macro-particle'. This is important for the comparison to particle-tracking calculations and give a rich source of information e.g. on local betatron phase advance, chromaticity and several non-linear quantities. On the technical side of most applications, a broadband signal amplification chain and fast digitalization is required for this mode. An appro-

priate trigger ensures the digitalization of each bunch; this trigger could be generated by hardware, but in modern applications this might be substituted by some type of software algorithms.

– In a synchrotron lattice parameters, like tune and chromaticity, are normally defined as a quantity per turn. They can precisely be determined using BPMs read on a **turn-by-turn** basis. E.g. the beam can be excited to coherent betatron oscillations and the position can be read by the BPM, the corresponding Fourier transformation results in the tune value. An appropriate hard- or software trigger is required for this mode.
– To determine the **closed orbit** within a synchrotron, the beam position is evaluated with a time resolution much longer than revolution time within this synchrotron. The resolution of the position reading is much higher than for the single bunch reading for two reasons: Firstly, coherent betatron oscillations are averaged out by this long observation time. Secondly, due to the much lower bandwidth of the electronics the noise contribution, as mainly given by thermal noise, is drastically reduced. A spatial resolution down to a μm or 10^{-5} of the pipe aperture (which always is smaller) can be achieved for observation time in the order of seconds. The related electronics is discussed in Chapter 7.

The position reading is not only used for monitoring, but at many facilities for position correction as well. Quite different reaction times are realized, from a bunch-by-bunch feedback to cure fast instabilities up to precise closed orbit corrections on a time scale of several seconds. As for the position measurement, fast reaction time counteracts high position resolution and an adequate compromise has to be found. Different feedback systems are discussed as a separate topic within this CAS Proceedings.

But BPMs are not only used for the determination of the beam center, but also for the observation of the longitudinal behavior i.e. the bunch shape recorded as a function of time. Frequent applications are:

– The bunch shape is recorded with high time resolution using broadband processing electronics. In particular, for a proton synchrotron with a bunch frequency below several 10 MHz, the bandwidth of the BPM and the processing electronics is large enough to image the bunch shape during injection, acceleration and eventual bunch manipulations or reorganization. For a synchrotron it is sufficient to have one device for this purpose, because a typical variation of the bunch shape occurs within the time scale of one period of the synchrotron oscillation, which is much longer than the revolution time. To achieve the required large bandwidth a Wall Current Monitor or a fast Current Transformer is better suited than linear-cut BPMs.
– At a proton Linac the average beam velocity has to be determined with high accuracy. From the time-of-flight of a dedicated bunch between two BPMs the beam velocity is calculated, an accuracy of $\Delta v/v \simeq 10^{-4}$ can be achieved. The same BPM installation is used for this velocity and the position measurement.
– The signal from a BPM can serve as a relative measure for the beam current. This method is more sensitive as can be provided by a dc current transformer. Using a narrowband filtering of the signal from the BPM at one of the bunch harmonics, the thermal noise contribution can be drastically reduced. Due to the evaluation at one frequency band only, the evaluation becomes bunch shape dependent and results in the ability of a relative current measurement only.

In this paper the general properties of a BPM installation are described for typical applications at standard accelerators. Further details and quantitative expression for the BPM properties can be found in other review articles as Refs. [1]–[7].

2 Signal treatment for capacitive BPMs

2.1 General formalism

A capacitive pick-up consists of a plate or a ring inserted in the beam pipe, as shown in Fig. 3. Here the induced image charge of the beam is coupled via an amplifier for further processing. The plate at a distance a from the beam center has an area of A and a length in longitudinal direction of l. The current I_{im} driven by the image charge Q_{im} is

$$I_{im}(t) \equiv \frac{dQ_{im}}{dt} = \frac{A}{2\pi a l} \cdot \frac{dQ_{beam}(t)}{dt}. \tag{2}$$

Having a beam with velocity β we can write for the derivative of the beam charge $dQ_{beam}(t)/dt$

$$\frac{dQ_{beam}(t)}{dt} = \frac{l}{\beta c}\frac{dI_{beam}}{dt} = \frac{l}{\beta c} \cdot i\omega I_{beam}(\omega) \tag{3}$$

where the beam current is expressed in the frequency domain as $I_{beam} = I_0 e^{i\omega t}$. (More precisely: The derivative of a function df/dt can be expressed as a multiplication of its Fourier transformation $\tilde{f}(\omega)$ with $-i\omega$.) As the signal source one uses the voltage drop at a resistor R

$$U_{im}(\omega) = R \cdot I_{im}(\omega) = Z_t(\omega,\beta) \cdot I_{beam}(\omega) \tag{4}$$

For all types of pick-up plates, the general quantity of longitudinal transfer impedance $Z_t(\omega,\beta)$ is defined in the frequency domain according to Ohm's law. It describes the effect of the beam on the pick-up voltage and it is dependent on frequency, on the velocity of the beam particles β and on geometrical factors. It is very helpful to make the description in the frequency domain, where the independent variable is the angular frequency ω, related to the time domain by Fourier transformation.

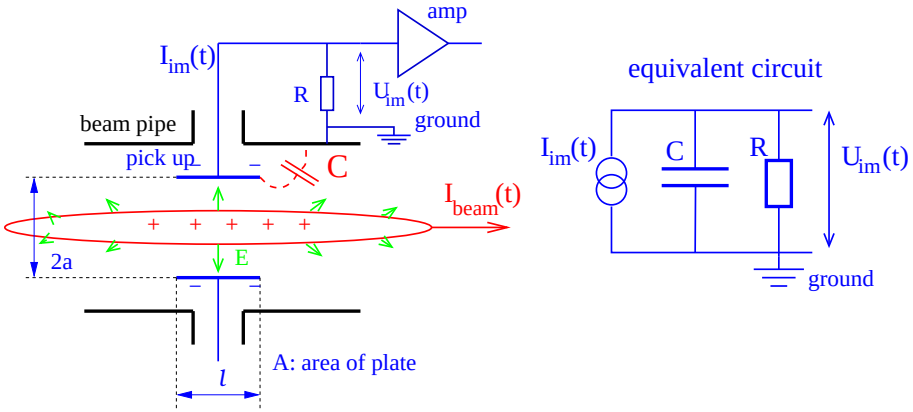

Fig. 3: Scheme of a pick-up electrode and its equivalent circuit.

The capacitive pick-up of Fig. 3 has a certain capacitance C, as given by the distance of the plate with respect to the beam pipe and a capacitance contributed by the cable between the plate and the amplifier input. This amplifier has a input resistor R. Using a current source to model the beam and the parallel connection of the equivalent circuit one can write its impedance Z as

$$\frac{1}{Z} = \frac{1}{R} + i\omega C \quad \Longleftrightarrow \quad Z = \frac{R}{1+i\omega RC} \tag{5}$$

therefore the transfer function of the pick-up is

$$U_{im} = \frac{R}{1+i\omega RC} \cdot I_{im} = \frac{1}{\beta c}\frac{1}{C}\frac{A}{2\pi a}\frac{i\omega RC}{1+i\omega RC} \cdot I_{beam} \equiv Z_t(\omega,\beta) \cdot I_{beam} \quad . \tag{6}$$

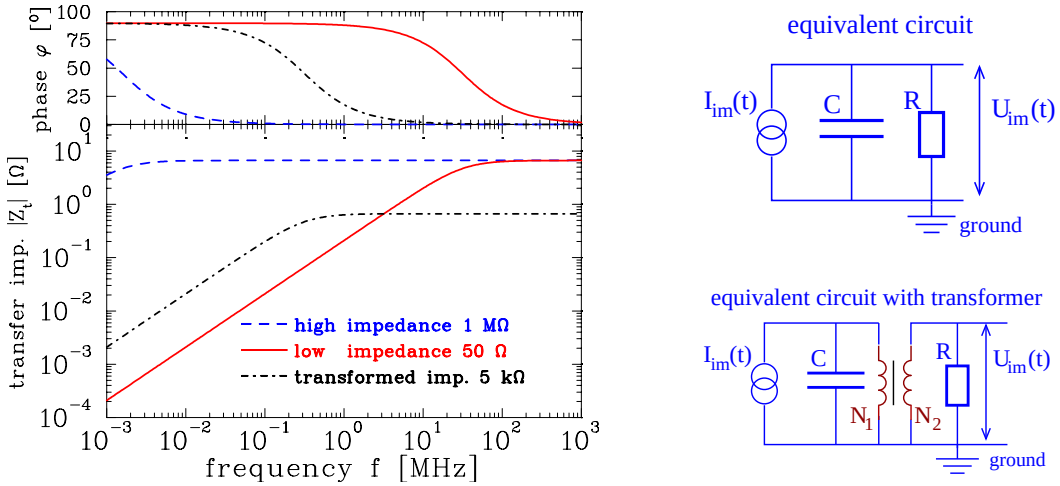

Fig. 4: Absolute value and phase of the transfer impedance for a $l = 10$ cm long round pick-up with a capacitance of $C = 100$ pF and an ion velocity of $\beta = 50\%$ for high (1 MΩ) and low (50 Ω) input impedance of the amplifier. The third curve is a $N_1 : N_2 = 30 : 3$ coupling by a transformer with primary windings N_1 and secondary windings N_2. On the right, the equivalent circuit with and without transformer coupling is shown.

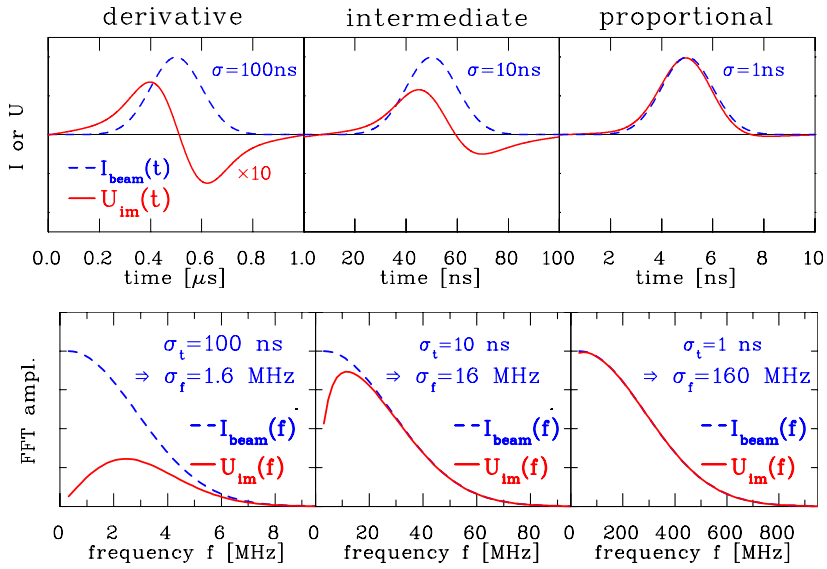

Fig. 5: Top: Simulation of the image voltage $U_{im}(t)$ for the values of the pick-up used in Fig. 4 terminated with $R = 50\,\Omega$ for three different bunch lengths with σ_t of 100 ns, 10 ns and 1 ns for a Gaussian distribution, respectively. Bottom: Fourier spectrum of the bunches and image voltages $\tilde{U}_{im}(\omega)$ for the three cases. The cut-off frequency is $f_{cut} = 32$ MHz. (The bunch length of $\sigma_t = 1$ ns is artificially short for a proton synchrotron.)

This is a description of a first order highpass filter with a cut-off frequency $f_{cut} = \omega_{cut}/2\pi = (2\pi RC)^{-1}$. For the case of the so called linear-cut BPM used at proton synchrotrons (see below), a typical value of the capacitance is $C = 100$ pF with a length of $l = 10$ cm. For this type the highpass characteristic is shown in Fig. 4 with a 50 Ω, a high impedance 1 MΩ amplifier input resistor as well as an intermediate value of 5 kΩ over the interesting frequency range. In the figure the absolute value

$$|Z_t| = \frac{1}{\beta c}\frac{1}{C}\frac{A}{2\pi a}\frac{\omega/\omega_{cut}}{\sqrt{1+\omega^2/\omega_{cut}^2}} \quad \text{and the phase relation} \quad \varphi = \arctan\left(\omega_{cut}/\omega\right) \tag{7}$$

is shown. A pick-up has to match the interesting frequency range, which is given by the acceleration frequency and the bunch length. As extremes we can distinguish two different cases for the transfer impedance, namely:

– **high frequency range** $f \gg f_{cut}$**:** Here we have

$$Z_t \propto \frac{i\omega/\omega_{cut}}{1+i\omega/\omega_{cut}} \longrightarrow 1 \quad . \tag{8}$$

The resulting voltage drop at R is for this case

$$U_{im}(t) = \frac{1}{\beta c C} \cdot \frac{A}{2\pi a} \cdot I_{beam}(t) \quad . \tag{9}$$

Therefore the pick-up signal is a direct image of the bunch time structure without phase shift, i.e. $\varphi = 0$. To get a low cut-off frequency $f_{cut} = (2\pi RC)^{-1}$ of typically ~ 1 kHz, high impedance input resistors are used to monitor long bunches, e.g. in proton synchrotrons. The calculated signal shape is shown in Fig. 5, right.

– **low frequency range** $f \ll f_{cut}$**:** Here the transfer impedance is

$$Z_t \propto \frac{i\omega/\omega_{cut}}{1+i\omega/\omega_{cut}} \longrightarrow i\frac{\omega}{\omega_{cut}} \quad . \tag{10}$$

The voltage across R is in this case

$$U_{im}(t) = \frac{R}{\beta c} \cdot \frac{A}{2\pi a} \cdot i\omega I_{beam} = \frac{R}{\beta c} \cdot \frac{A}{2\pi a} \cdot \frac{dI_{beam}}{dt} \tag{11}$$

using again the frequency domain relation $I_{beam} = I_0 e^{i\omega t}$. The measured voltage is proportional to the derivative of the beam current. This can also be understood from the phase relation of the highpass filter in Fig. 4, where a phase shift of 90^o corresponds to a derivative. The signal is bipolar, as shown in Fig. 5, left.

The signal at the amplifier output depends on the frequency range as compared to the cut-off frequency. In general the signal shape can be calculated using the transfer impedance concept by the following steps:

– The beam current $I_{beam}(t)$ is Fourier transformed yielding $\tilde{I}_{beam}(\omega)$.
– It is multiplied by $Z_t(\omega)$ yielding the frequency dependent voltage $\tilde{U}_{im}(\omega) = Z_t(\omega) \cdot \tilde{I}_{beam}(\omega)$.
– To get back the time dependent signal the inverse Fourier transformation is applied yielding the signal $U_{im}(t)$.

Beside the time evolution of the Gaussian beam bunches of width σ_t and the resulting signal voltage the frequency spectrum is shown in Fig. 5: The width of the transformed beam current $\tilde{I}_{beam}(\omega)$ in frequency domain is given by $\sigma_f = (2\pi\sigma_t)^{-1}$ in case of a Gaussian distribution. If the bunch spectrum ranges far above the cut-off frequency the multiplication by the transfer impedance $Z_t(\omega)$ does not change the spectral shape of image voltage $\tilde{U}_{im}(\omega)$ significantly as shown in Fig. 5, right. The inverse transformation leads to a proportional image voltage $U_{im}(t)$ as discussed for the first case above. For the second case, the main contribution of the frequency spectrum is below the cut-off frequency, therefore the multiplication by $Z_t(\omega)$ leads to a strong modification of the spectrum as shown in Fig. 5, left. The inverse Fourier transformation leads to the described behavior of $U_{im}(t) \propto dI/dt$. This type of calculation can be performed for any given bunch length; an example is plotted in the center part of Fig. 5: The main frequency components are in the same band as given by the cut-off frequency of the BPM leading to a significant modification of the image voltage spectrum $\tilde{U}_{im}(\omega)$. The resulting time evolution of $U_{im}(t)$, called intermediate case, shows a more complex behavior with some proportional and some differentiating components. For the signal calculation for these parameters, the full calculation via Fourier transformation is required.

With respect to the different limits of the transfer impedance above, two important applications are discussed for illustration:

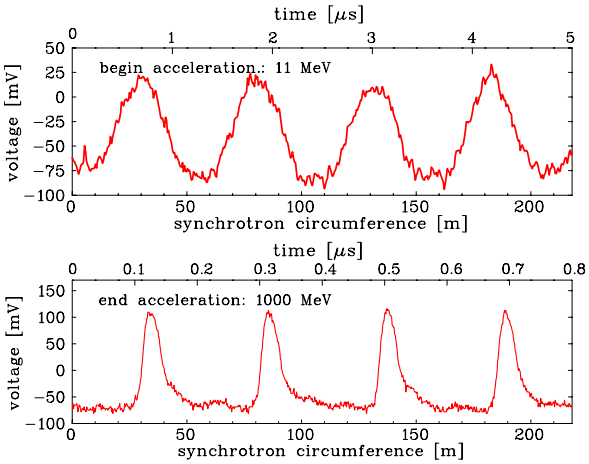

Fig. 6: Bunch signals from a linear-cut BPM with 1 MΩ termination. The upper curve shows the bunches along the synchrotron circumference at the beginning of acceleration, the lower curve at final energy. Note the different time scales on top of the plots.

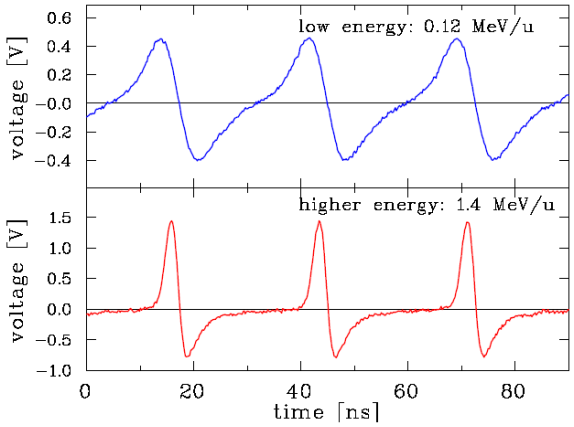

Fig. 7: Bunch signals from a button BPM with 50 Ω termination for 0.12 MeV/u (top) and 1.4 MeV/u (bottom) energy at the GSI-LINAC. The acceleration frequency is 36 MHz.

– **Range $f \gg f_{cut}$ realized by a *low* f_{cut} due to high impedance:**
In a proton synchrotron a low acceleration frequency 1 MHz $< f_{acc} <$ 30 MHz is used, resulting in bunches of several meters in length. In these machines, large apertures are necessary of typically $a = 10$ cm, which lowers the transfer impedance due to $Z_t \propto 1/a$. To get a larger sensitivity, the length of the BPM in beam direction is typically $l \sim 10$ cm due to $Z_t \propto l$. Note that the BPM length is still much shorter than the bunch length. To have a flat frequency response, i.e. a large bandwidth, a low $f_{cut} = (2\pi RC)^{-1}$ is used by feeding the signal into a high impedance FET transistor as first step of the amplifier. A bandwidth of the amplifier circuit of 100 MHz can be reached. To prevent from signal degeneration due to the limited amplifier bandwidth the application of high impedance amplifiers is restricted to proton synchrotrons with less than ~ 10 MHz acceleration frequency. As shown in Fig. 6 a direct image of the bunch is seen in this case.

– **Range $f \ll f_{cut}$ realized by a high f_{cut} due to 50 Ω impedance:**
At LINACs and electron synchrotrons, the bunches are short, in the mm range, due to the higher acceleration frequencies (100 MHz $< f_{acc} <$ 3 GHz). A 50 Ω termination is used to prevent reflections and to get smooth signal processing with a large bandwidth up to several GHz. The short l, and therefore a lower capacitance C of typically 1 to 10 pF, and the $R = 50$ Ω leads to a high f_{cut} in the range of several GHz and differentiated bunch signals are recorded as displayed in Fig. 7.

2.2 Application: Signal behavior for linear-cut BPM using transfer impedance Z_t concept

In the previous section, the transfer impedance Z_t was discussed for a single bunch passage only, which might be realized at transfer-lines between synchrotrons. But most other accelerators deliver a train of bunches separated by the time $t_{acc} = 1/f_{acc}$ as given by the acceleration frequency f_{acc} (assuming that all buckets are filled). As an example of transfer impedance properties and the resulting image voltage $U_{im}(t)$ behavior, the application for a typical linear-cut BPM used at proton synchrotrons is discussed here, see Chapter 3 for more details concerning this BPM type. The following values are used: The length in beam direction is $l = 10$ cm; the distance of the plates from the beam center is $a = 5$ cm covering the full circumference; the capacitance is $C = 100$ pF; these are the same parameters as used for the transfer impedance Z_t shown in Fig. 4. For this example we assume a synchrotron, where the acceleration is performed by $f_{acc} = 1$ MHz acceleration frequency, a revolution time of 8 μs and an

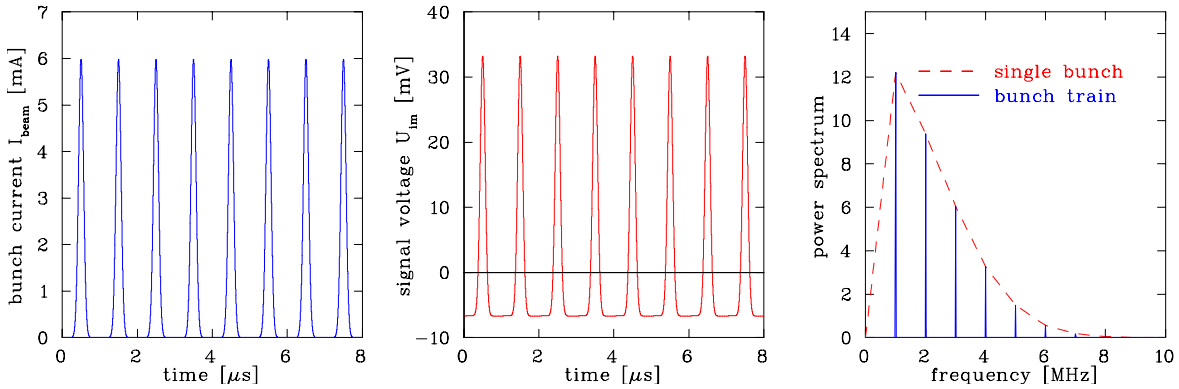

Fig. 8: Signal simulation for 1 MΩ termination of a BPM, see text for further parameters. Left: Beam current, middle: signal voltage , right: frequency spectrum of the signal voltage $\tilde{U}_{im}(f)$.

average current of 1 mA. In parts of the plots, the injection is performed in such a way that only 6 of 8 buckets are filled. The beam has a velocity of $\beta = 50$ % and a bunch duration of $\sigma_t = 66$ ns for a Gaussian distribution, corresponding to a bunch length of $\sigma_l = 10$ m, i.e. much longer than the BPM length of typically 10 cm. The following calculations use the concept of frequency dependent transfer impedance.

High impedance termination: In Fig. 8 a high impedance termination of $R = 1$ MΩ is chosen for the BPM signals leading to the highpass cut-off frequency $f_{cut} = (2\pi RC)^{-1} = 1.6$ kHz. The signal shape for $U_{im}(t)$ is proportional to the beam current $I_{beam}(t)$ with the proportional constant $Z_t \simeq 5\,\Omega$. However, the signal voltage shows some negative values, the so called baseline shift. Due to the BPM's high-pass characteristic any dc-signal part is disregarded by the BPM. The unipolar beam current is therefore transformed to an ac-signal with the condition, that the integral over one turn is zero, i.e. the baseline is lowered to a value in a way to counteract the positive signal strength; note that the value of the baseline depends on the bunch width. The frequency spectrum of this periodic signal is composed of lines at the acceleration frequency and its harmonics. In other words, the signal power is concentrated in narrow frequency bands separated by the acceleration frequency. It is quite common for the position evaluation to use only one of these frequency bands with high power density e.g. by filtering or narrowband processing to suppress broadband noise contributions, see Chapter 7. The envelope of these lines is given by the Fourier transformation of the single bunch current multiplied by the frequency dependent transfer impedance. For the bunch duration σ_t of this example, the maximum frequency is at about 10 times the acceleration frequency. For the layout of a broadband electronics it is reasonable to enlarge the bandwidth up to at least the tenth harmonics to record the full signal shape and its full power spectrum, correspondingly. Using a Gaussian bunch shape the relation of the Fourier transformation $\sigma_f = (2\pi\sigma_t)^{-1}$ can be used for the bandwidth estimation. Note that for non-Gaussian bunch shapes of the same σ_t, the frequency spectrum continues to higher values.

50 Ω termination: It is quite common in rf-technologies to use 50 Ω terminations for signal transmission, therefore a related impedance for the BPM amplifier input seems to be adequate. The signal shape is depicted in Fig. 9. However, for the parameters of this example a termination with a 50 Ω resistor leads to a signal of differentiating shape with a voltage amplitude decrease by a factor $\simeq 20$ compared to the high impedance termination. This is caused by the $f_{cut} = 32$ MHz BPM's high pass characteristic, which is larger than the relevant frequencies as given by the single bunch envelope, see Fig. 9, right. This low signal amplitude is the reason, why at proton synchrotrons a higher impedance termination is preferred.

Transformer coupling: A high impedance coupling delivers a larger signal strength, but as it can be seen in Eq. 9, the signal strength decreases with the capacitance. Because regular coaxial cables have

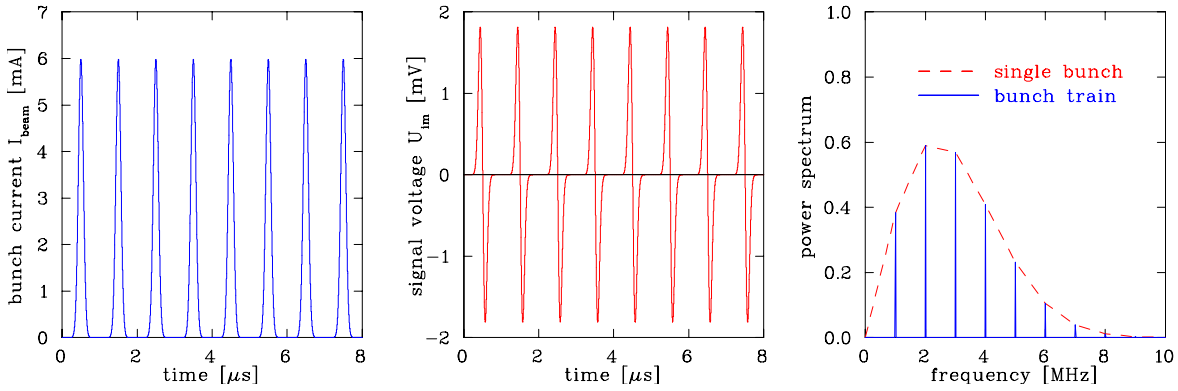

Fig. 9: Signal simulation for 50 Ω termination of a BPM, see text for further parameters.

a capacitance of about 100 pF per meter, only short cable between the BPM plates and the amplifier are allowed for this case. Sometimes cables of several meter length are required and for that an impedance matching to 50 Ω close to the BPM plates by a passive transformer is necessary. The realizations for winding rations of typically $N_1 : N_2 \simeq 6 : 1$ to $20 : 1$ are described e.g. in [8]. The $R_{ampl} = 50\ \Omega$ input impedance of the amplifier or the cables are transformed proportionally to the square of the winding ratio $R_{eff} = (N_1/N_2)^2 \cdot R_{ampl}$, leading to an effective impedance of about $R_{eff} = 1 - 10$ kΩ for the BPM. The transfer impedance for an impedance of $R_{eff} = 5$ kΩ corrsponding to a highpass cut-off frequency of $f_{cut} = 320$ kHz is shown in Fig. 4 together with the equivalent circuit of this arrangement. Because the voltage ratio above the cut-off frequency for a transformer is given by $U_2/U_1 = N_2/N_1 = 3/30$, the signal strength U_2 is lower by this factor compared to the high impedance case. However, the thermal noise is lower compared to the high impedance termination due to the scaling of the effective voltage $U_{eff} \propto \sqrt{R}$; this topic is discussed in Chapter 7.1. The cut-off frequency of $f_{cut} = 320$ kHz leads to a deformation of the signal as depicted in Fig. 10. In particular, the baseline is not stable as for the high impedance case, but approaches a zero value within a time constant given by $t_{cut} \simeq (3 \cdot f_{cut})^{-1} = 1\ \mu$s, leading to non-constant values between the bunches. In the plot the behavior is depicted for the case of empty buckets i.e. only part of the synchrotron is filled with particles. The frequency spectrum is more complex due to the break of periodicity by the empty buckets.

Signal shape using filters: The concept of transfer impedance can not only be used to calculate the BPM characteristics but can serve as an estimation for the signal conditioning by the processing analog electronics as well. Filtering is important to suppress unwanted frequency components and to restrict the bandwidth dependent noise. A mathematically simple filter is the so called Butterworth filter of n^{th}-order with a frequency response for the lowpass part $|H_{low}(\omega)| = 1/\sqrt{1 + (\omega/\omega_{low})^{2n}}$ and

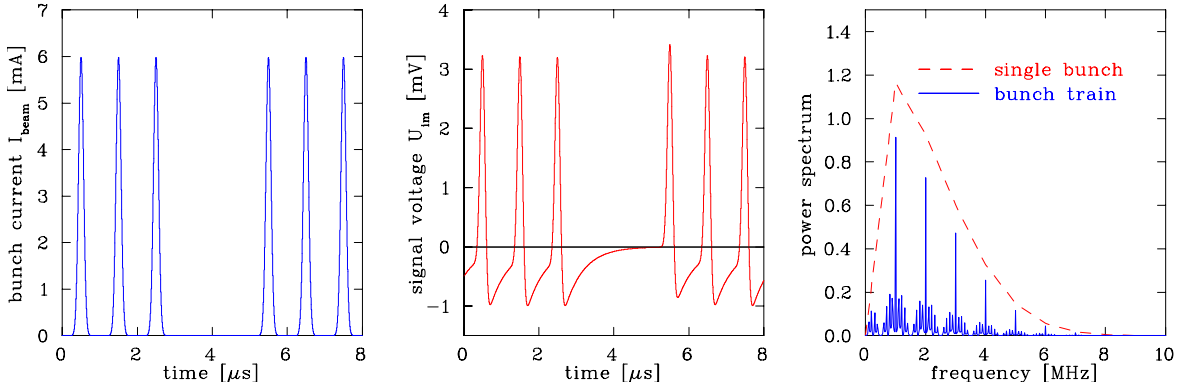

Fig. 10: Signal simulation for 5 kΩ termination of a BPM, see text for further parameters.

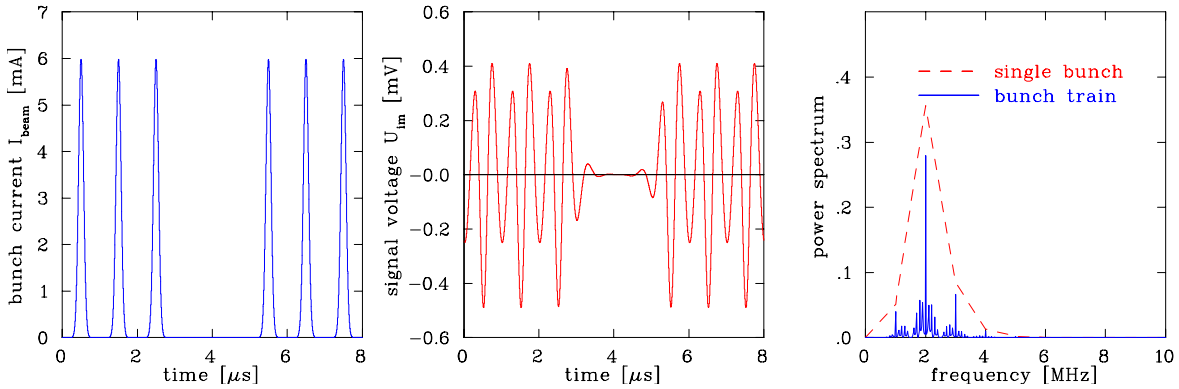

Fig. 11: Signal simulation for 5 kΩ termination of a BPM followed by a 4^{th} order Butterworth bandpass filter at the 2^{nd} harmonics of the acceleration frequency, see text for further parameters.

the highpass frequency response $|H_{high}(\omega)| = (\omega/\omega_{high})^n/\sqrt{1+(\omega/\omega_{high})^{2n}}$ at the cut-off frequencies $f_{low} = \omega_{low}/2\pi$ and $f_{high} = \omega_{high}/2\pi$ for the lowpass and highpass filter, respectively [9]. A bandpass filter is modeled as the product $H_{band}(\omega) = H_{low}(\omega) \cdot H_{high}(\omega)$ taking amplitude and phase response into account, i.e. regarding $H(\omega)$ as a complex function in mathematical sense. The action of such a 4^{th} order filter with cut-off frequencies $f_{low} = 2.2$ MHz and $f_{high} = 1.8$ MHz is shown in Fig. 11. As it can be seen from the frequency spectrum only the region around the cut-off frequencies is transmitted through the filter. In time domain, the action results in a certain oscillation or 'ringing', because the Gaussian bunch shape cannot be reconstructed by the limited frequency spectrum. It is worth mentioning that the properties for the final signal shape including the frequency response of amplifiers H_{ampl}, filters H_{filter} and cables H_{cable} etc. can be estimated by multiplying the related transfer impedance and frequency responses as complex functions via

$$Z_{tot}(\omega) = H_{cable}(\omega) \cdot H_{ampl}(\omega) \cdot H_{filter}(\omega) \cdot .... \cdot Z_t(\omega) \tag{12}$$

resulting in the time and frequency domain signal behavior. The properties of digital filters better suited for these applications are described in textbooks on Digital Signal Processing [9, 10] as well as the methods for signal treatment in time or frequency domain.

The discussion above took only the signal strength into account, but the noise contribution is another issue as discussed in Chapter 7.1. The properties of a linear-cut BPM were derived here as an example, but the same type of calculation can be performed for other types of BPMs, see e.g. [2, 11] for a button BPM application.

2.3 Position measurement by a BPM

In the description above the signal properties from an insulated plate covering the full circumference were discussed. However, the most frequent application of BPMs is the measurement of the beam's center-of-mass with respect to the center of the beam pipe. For a capacitive coupling, this is performed using four isolated plates by determining the difference voltage $\Delta U_x = U_{right} - U_{left}$ and $\Delta U_y = U_{up} - U_{down}$ of opposite plates for horizontal and vertical direction, respectively. The closer distance to one of the plates leads to a higher image current, which is called 'proximity effect' and is schematically shown in Fig. 12. The signal strength on the plate can be estimated to first order using the transfer impedance as given in Eq. 7 with the area A of the single plate. The horizontal displacement x can be obtained by a normalization to the sum signal $\Sigma U_x = U_{right} + U_{left}$ as

$$x = \frac{1}{S_x} \cdot \frac{U_{right} - U_{left}}{U_{right} + U_{left}} + \delta_x \equiv \frac{1}{S_x} \cdot \frac{\Delta U_x}{\Sigma U_x} + \delta_x \quad \text{(horizontal)} \tag{13}$$

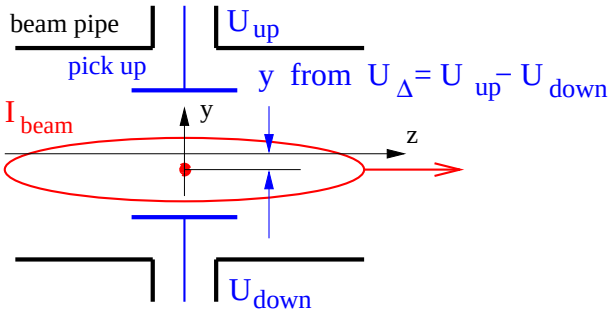

Fig. 12: Proximity effect for the BPM's vertical plane.

which is independent of the beam current. For the vertical plane the position y is given by

$$y = \frac{1}{S_y} \cdot \frac{U_{up} - U_{down}}{U_{up} + U_{down}} + \delta_y \equiv \frac{1}{S_y} \cdot \frac{\Delta U_y}{\Sigma U_y} + \delta_y \quad \text{(vertical)}. \tag{14}$$

The proportional constant S_x respectively S_y between the measured voltage difference and the beam displacement is called **position sensitivity** and its unit is $S = [\%/mm]$. It is possible that this constant additionally depends on the beam position itself, corresponding to a non-linear voltage response for a large beam displacement, which is demonstrated for button BPMs in Chapter 4. If the position sensitivity is given as a pure number, it refers to the value of the central region. In contrast to button BPMs, the realization by the linear-cut design is optimized for a linear position sensitivity S over a large displacement range as discussed in Chapter 3. A deviation of the electrical center, as given by equal output voltages on both plates, and the geometrical center is possible, which is considered by the offset correction δ having the unit $\delta = [mm]$. It is not necessarily the case that the position sensitivity S and the offset δ are equal for the horizontal and vertical plane, because the BPM installation might be non-symmetric for both directions and the surrounding close to the BPM might modify the propagation of the beam's electro-magnetic field. Moreover, due to the capacitive coupling, a frequency dependence of the position sensitivity S and the offset δ is possible and has to be minimized by a good mechanical design to prevent from complicated corrections. The definition of Eqs. 13 and 14 holds for other than capacitive BPMs, as well.

For typical beam displacements less than 1/10 of the beam pipe aperture, the difference ΔU is lower by about this factor compared to the sum voltage ΣU i.e.

$$\text{typically} \quad \Delta U < \frac{\Sigma U}{10} \quad . \tag{15}$$

Sensitive signal processing is required for the difference voltage to achieve a sufficient signal-to-noise ratio. This concerns the usage of low noise amplifiers, which have to be matched to the signal level. Sometimes difference and sum voltage are generated by analog means using a transformer with differential windings for the low frequency range at proton synchrotrons or $\Delta - \Sigma$ hybrids for high frequency applications. For these cases the difference voltage can be more amplified than the sum signal (typically by 10 dB equals to a factor of 3 for the voltage amplification) to match the optimal signal level for the successive electronics or analog-digital conversion. The most effective noise reduction is achieved by a limitation of the signal processing bandwidth, because the thermal noise voltage U_{eff} at a resistor R scales with the square root of the bandwidth Δf as $U_{eff} = \sqrt{4 k_B T R \Delta f}$ with k_B being the Boltzmann constant and T the temperature. As shown above in Chapter 2.2 the signal power is concentrated in bands given by the acceleration frequency f_{acc}. The bandwidth limitation is performed by bandpass filtering at a harmonics of this frequency or mixing with the accelerating frequency in the narrowband processing as discussed in Chapter 7.

2.4 Characteristics for position measurement

For the characterization of a position measurement system several phrases are frequently used, which are compiled in the following:

Position sensitivity: It is the proportional constant between the beam displacement and the signal strength. It is defined by the derivative

$$S_x(x) = \frac{d}{dx}\left(\frac{\Delta U_x}{\Sigma U_x}\right) = [\%/\text{mm}] \text{ (linear)} \qquad S_x(x) = \frac{d}{dx}\left(\log\frac{U_{right}}{U_{left}}\right) = [\text{dB/mm}] \text{ (logarithmic)} \quad (16)$$

for the horizontal direction and for the vertical direction, correspondingly. The unit is $S = [\%/\text{mm}]$ in case of linear processing or $S = [\text{dB}/\text{mm}]$ in case of logarithmic processing (the logarithmic processing is described in Chapter 7.3) . For small displacements a constant value is expected. For larger displacements the horizontal sensitivity S_x might depend on beam position in horizontal direction, called non-linearity, and additionally in vertical direction, called horizontal-vertical coupling. Moreover, it might depend on the evaluation frequency. In the most general case the position sensitivity $S(x,y,\omega)$ is a function of horizontal and vertical displacement as well as frequency. Often the inverse of S is used having the abbreviation $k = 1/S$ and is given in the unit of $k = [mm]$.

Accuracy: It refers to the ability of position reading relative to a mechanical fix-point or to any other absolutely known axis e.g. the symmetry axis of a quadrupole magnet. The accuracy is mainly influenced by the BPM's mechanical tolerances as well as the long-term stability of the mechanical alignment. For cryogenic installations the mechanical position reproducibility after cool-down cycles influences the accuracy. Beside these mechanical properties, it is influenced by electronics properties like amplifier drifts, noise and pickup of electro-magnetic interference. By calibrating the electronics in regular time intervals long-term drifts can be compensated. The digitalization leads to a granularity of values, which might limit the reachable accuracy; for modern installations this limitation is compensated by improved ADC technologies.

Resolution: It refers to the ability for measuring small displacement variations. In contrast to the accuracy relative values are compared here. In most cases, the resolution is much better than the accuracy. It depends strongly on the measurement time because averaging procedures can exceed the accuracy by a factor of 100. Typical values for the resolution for a broadband, single bunch reading is 10^{-3} of the beam pipe radius or roughly $\simeq 100$ μm. For averaged readings on typical time scale of 10 to 1000 ms, a resolution of 10^{-5} of the beam pipe radius or roughly $\simeq 1$ μm can be reached. As for the accuracy, it depends on the electronics noise contribution as well as short-term and long-term drifts.

Analog bandwidth: The lower and upper cut-off frequency of the analog electronics have to be matched to the frequency spectrum delivered by the bunched beam. For noise reduction, the bandwidth can be limited by analog filters.

Acquisition bandwidth: It refers to the frequency range over which the beam position is recorded and should be matched to the analog bandwidth. For monitoring fast changes of beam parameters a much larger bandwidth is required, resulting in a lower position resolution. The same is valid for short beam deliveries, e.g. in transport lines, preventing from averaging. The bandwidth can be restricted to achieve a high resolution in case of slow varying beam parameters, as it is the case for the analog narrowband processing with multiplexing described in Chapter 7.4.

Real-time bandwidth: The data rate of producing an analog or digital position signal with predictable latency to be used e.g. by an orbit feedback system is characterized by this quantity.

Dynamic range: It refers to the range of beam current for which the system has to respond to. In most cases the signal adoption is done by a variable gain amplifier at the input stage of the electronics processing chain. Within the dynamic range, the position reading should have a negligible dependence with respect to the input level.

Signal-to-noise ratio: It refers to the ratio of wanted signal to unwanted noise. An unavoidable contribution is given by thermal noise. Cooling of the first stage amplifier reduces this thermal noise. Other sources, like electro-magnetic pickup or ground-loops can contribute significantly to an unwanted signal

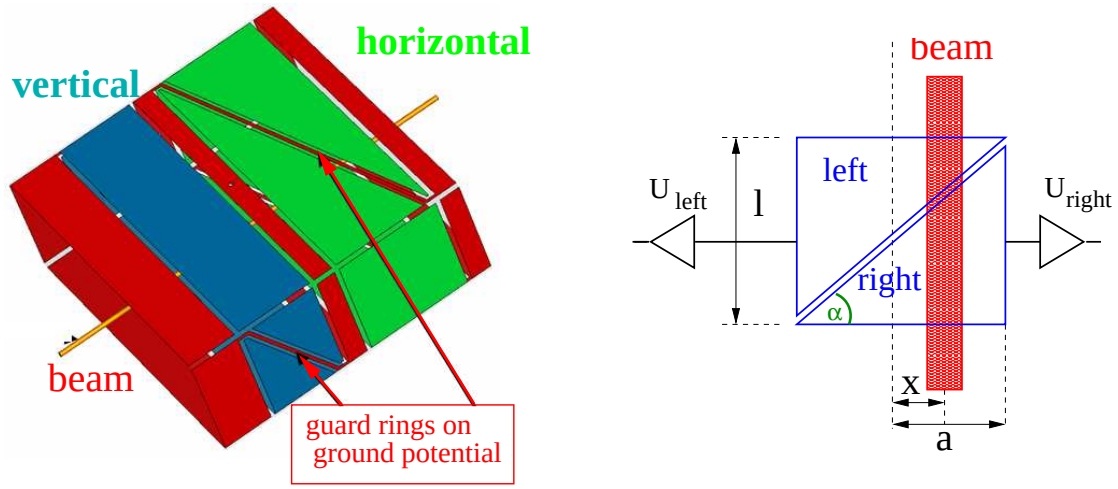

Fig. 13: An example of a rectangular electrode arrangement for a linear-cut BPM and the scheme for position determination.

disturbance and are incorporated in this phrase even though they are not caused by noise. Careful shielding and grounding is required to suppress these disturbances.
Detection threshold: It refers to the minimal beam current for which the system delivers a usable information. It is limited by noise contributions. Sometimes this quantity is called signal sensitivity.

3 Linear-cut BPM

At proton synchrotrons the linear-cut or shoe-box BPM type is often installed due to its excellent position linearity and large signal strength. The transfer impedance $|Z_t|$ above the cut-off frequency is typically 1 to 10 Ω. Basically, this type consists of consecutive plates surrounding the beam. A typical geometry for a rectangular realization is shown in Fig. 13, where the electrodes for the horizontal direction look like a piece of cake. In contrast to other BPM types, the signal strength is not related to proximity of the beam with respect to the BPM plates but is given by the fraction of beam coverage by the BPM electrodes. For a given beam displacement x the electrode's image voltage U_{im} is proportional to the length l of the beam projected on the electrode surface as shown for the horizontal direction in Fig 13, right. For triangle electrodes with half-aperture a one can write:

$$l_{right} = (a+x)\cdot\tan\alpha \quad \text{and} \quad l_{left} = (a-x)\cdot\tan\alpha \quad \Longrightarrow \quad x = a\cdot\frac{l_{right}-l_{left}}{l_{right}+l_{left}} \quad . \tag{17}$$

The position reading is linear and can be expressed by the image voltages as

$$x = a\cdot\frac{U_{right}-U_{left}}{U_{right}+U_{left}} \equiv \frac{1}{S_x}\cdot\frac{\Delta U_x}{\Sigma U_x} \quad \Longrightarrow \quad S_x = \frac{1}{a} \tag{18}$$

which shows that the position sensitivity for this ideal case is simply given by the inverse of the half-aperture.

This ideal behavior can nearly be reached, e.g. a position sensitivity up to $S_x \approx 90\%\cdot 1/a$ can be realized by a careful design [13]. As an example the position evaluation by a 3-dimensional Finite Element Method (FEM) calculation is depicted in Fig. 14 together with the geometry of the considered BPM. The position sensitivity is given by the slope of the difference-over-sum calculation as a function of beam displacement according to Eq. 16. For this simulation the beam center is swept in horizontal direction from $x = -60$ mm to $x = +60$ mm in steps of 20 mm and the reading of the horizontal BPM electrodes is plotted. These sweeps are performed with three different vertical beam positions, namely in the middle plane $y = 0$ and with $y = +20$ mm above as well as $y = -20$ mm below the BPM center. These

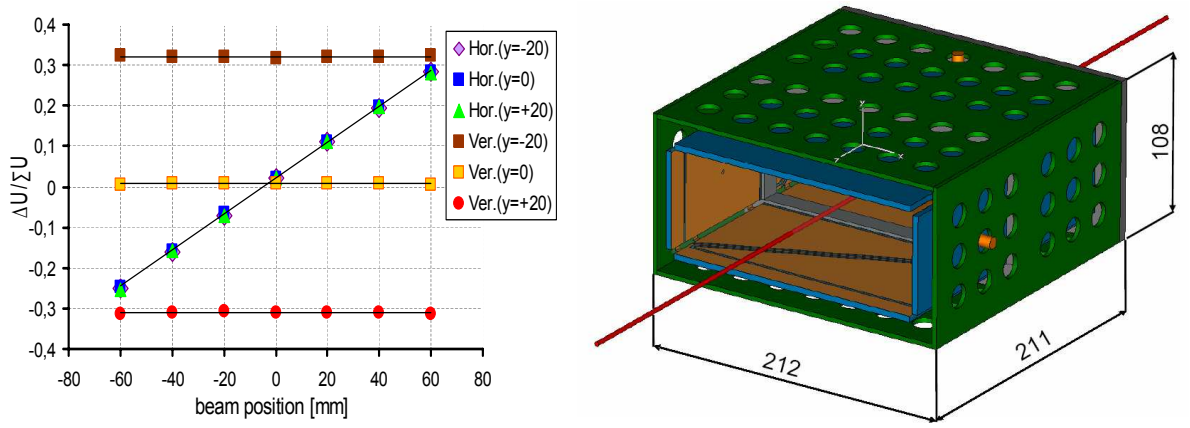

Fig. 14: Results of Finite Element Method calculations for the horizontal plane of a linear-cut BPM are shown left. The center of the simulated beam is swept in horizontal direction (curves with constant slope) and vertical direction (constant functions). The BPM geometry for these calculations is depicted right having a horizontal half-aperture of $a = 100$ mm. Due to the cross talk between the horizontal electrodes the sensitivity is only $S_x = 0.43/a$.

three curves coincide and show a nearly perfect linearity with less than 1% deviation from the linear fit. Additionally, three sweeps in vertical direction with constant position in x are shown in the figure, but there is no influence on the horizontal reading as the data points are located on the three lines parallel to the x-axis. This proves the linearity (sweep in x direction) and the absence of any horizontal-vertical coupling (sweep in y direction), which is a unique feature of these BPM types.

However, the properties of the ideal case can only be maintained by several precautions. The value of the position sensitivity is influenced by the capacitive coupling between the adjacent electrodes and an efficiently electrical separation between these electrodes is required, i.e. a reduction of the plates' cross talk. The coupling capacitance depends on the electrode's size, the width of the diagonal cut and the permittivity of the material used as the electrode support. For a BPM design based on metalized Al_2O_3 ceramics the permittivity is $\varepsilon_r \approx 9.5$ which leads to a coupling capacitance of about 10 pF. For such a BPM an additional separation region on ground potential (the so called guard ring) positioned in the diagonal cut area is required and visible in Fig. 13, left. The guard ring reduces the cross talk between adjacent electrodes by factor of three and, correspondingly, increases the position sensitivity by a factor of two [12]. If the BPM design is based on pure metallic electrodes the distance between adjacent plates cannot be increased above a critical value, otherwise the linearity is spoiled by field inhomogeneities within the gap.

The BPM electrodes are not symmetrical with respect to the beam direction which results in an asymmetry of the electric field at the adjacent electrode edges. Even a small asymmetry introduces a field inhomogeneity that leads to an offset of the geometrical center with respect to the electrical center, defined by a zero difference voltage $\Delta U = 0$. This offset is regarded by δ_x in Eq. 13 and can be as large as 10% of the BPM half-aperture a [13]. This fringe field contribution is minimized by sufficient long guard rings on ground potential located at the entrance and exit of the BPM to ensure identical environments on both sides. Moreover, the guard ring is required for and electrical separation of the horizontal and vertical BPM part, see also Ref. [15]. The influence of these distortions depends on the BPM's length and aperture. In extreme case for a short BPM with large aperture the reading might be dominated by this fringe field contribution [16, 17].

As it was already mentioned in Chapter 2.3 the position sensitivity can be frequency dependent. This is harmful for beams with varying bunch length during acceleration and possible bunch manipulations which lead to a varying frequency spectrum. The left part of Fig. 15 demonstrates the frequency dependence of the position sensitivity and offset for a BPM without a guard ring between the horizontal

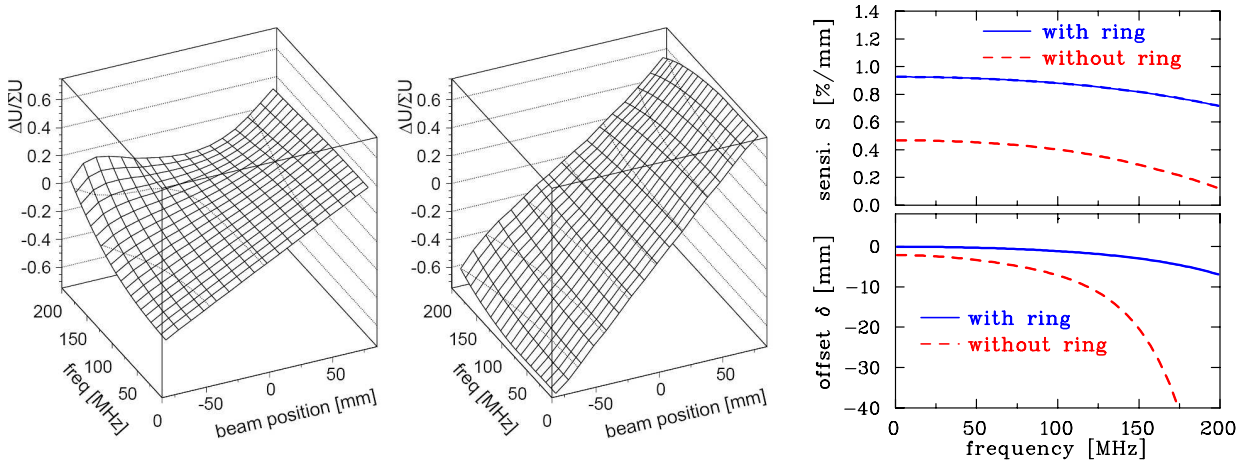

Fig. 15: The position signal as a function of displacement and frequency performed by Finite Element calculations for a linear-cut BPM without a guard ring is shown left. Inserting a guard ring the signal linearized (middle). The frequency dependence of the position sensitivity and offset for both cases is shown right, from [12].

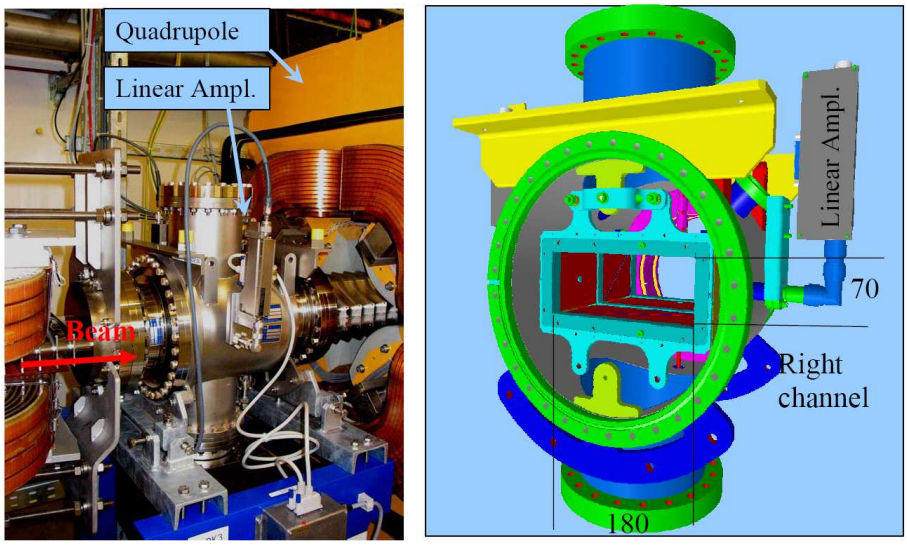

Fig. 16: Photo of a linear-cut BPM at the ion therapy facility HIT (left) and its technical drawing (right).

electrodes: Above 50 MHz the sensitivity decreases significantly and becomes nonlinear. This is caused by the frequency dependent capacitive coupling between the plates, at about 200 MHz this cross talk dominates the signal generation. The middle part of Fig. 15 shows corresponding result obtained for the same BPM but equipped with a guard ring. In this case the cross talk is avoided resulting in a factor twofold position sensitivity and a linear frequency behavior. The position sensitivity S, defined as the derivative for small beam displacements, and the offset δ according to Eq. 13 yield the frequency dependence which is depicted for both variants in Fig. 15, right. A linear frequency behavior of S and a small value of δ is a crucial design criterion to avoid systematic errors in the position reading.

At proton synchrotrons the acceleration frequency is typically a few MHz leading to a bunch length of about 10 m which is much longer than the BPM itself. Fig. 16 shows an example of such an installation. The rectangular shape and the required guard rings lead to a relatively complex mechanical realization of the BPM body. But the advantage of the position linearity and avoidance of horizontal-vertical coupling legitimates the related efforts.

Linear-cut BPMs must not necessarily have a rectangular cross section. It is only important that

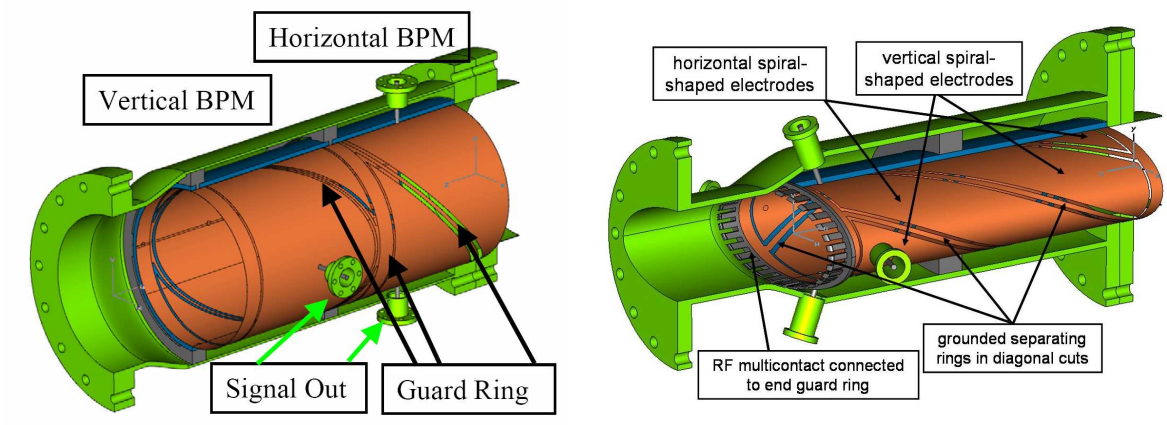

Fig. 17: Left: Linear-cut BPM in cylindrical geometry, Right: Wounded strip geometry, see [13, 14].

the projection of the cut between adjacent electrodes on the vertical and horizontal planes is a diagonal line. An example of a cylindrical BPM is shown in Fig. 17, left, which has comparable properties to the rectangular counterpart. An alternative geometry made of wounded strips is shown in Fig. 17, right. The advantage of this wounded strip geometry is the equal length and coupling capacitance for all electrodes. In addition such electrode configuration allows to mount all feed-through at the same distance from the point where electrodes are fixed to the BPM chassis as it is important for a cryogenic environment. However, one has to be cautious since the coupling between orthogonal electrodes leads to a significantly horizontal-vertical coupling [14]. A variation of this wounded strip geometry is discussed e.g. in [4].

4 Button BPM

Button BPMs consist of an insulated metal plate of a typical diameter from several mm to several cm. They are used at proton LINACs, cyclotrons as well as at all types of electron accelerators, where the acceleration frequency is in most cases 100 MHz $< f_{acc} <$ 3 GHz, which is higher as for proton synchrotrons. The length of the bunches is correspondingly shorter, becoming comparable to the length of typically 10 cm of a linear-cut BPM. Shorter intersections are required with the advantage of a compact mechanical realization. A typical installation is shown in Fig. 18, where the four buttons surround the beam pipe. With a short pin the pick-up plate is connected to a standard rf-connector outside the vacuum. The transition from the button plate to the connector as well as the ceramic support of the vacuum parts have to be designed for low signal reflection, which becomes important at the GHz frequency range. In particular, the signal path towards the analog electronics has to obey the coaxial 50 Ω matching. Due to the 50 Ω coupling, the derivative of the beam current is recorded as discussed for Eq. 11. The capacitance of a single button is in the order of 1 to 10 pF, leading to a highpass cut-off frequency of 0.3 to 3 GHz. Together with the typical size of Ø 5 to 20 mm the transfer impedance $|Z_t|$ above cut-off frequency is 0.1 to 1 Ω.

The small size of the button and the short vacuum feed-through allows for a compact installation and is one reason for large proliferation at many accelerators. The cost of a button BPM installation is much lower than of a linear-cut arrangement, which is an important aspect with regard to the large amount of BPM locations along the accelerator.

4.1 Circular arrangement of button BPM

In the following a model for the estimation of the position reading from the buttons is presented. This model is basically an electro-static assumption in a 2-dimensional geometry of a circular beam pipe, but it leads to results comparable with numerical FEM calculations. According to Fig. 19 we assume a thin, 'pencil' beam of current I_{beam} which is located off-center by the amount r at an angle θ. The wall current

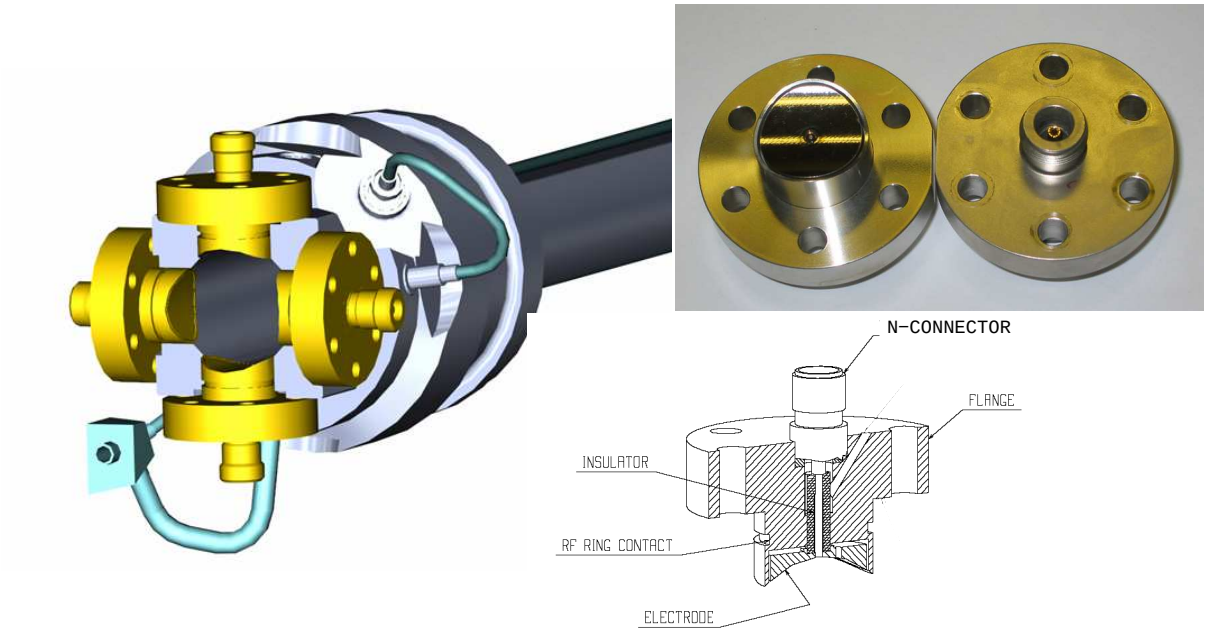

Fig. 18: Left: The installation of the curved Ø 24 mm button BPMs at the LHC beam pipe of Ø 50 mm, from [18]. Right: Photo of a BPM used at LHC, the air side is equipped with a N-connector as well as a technical drawing for this type.

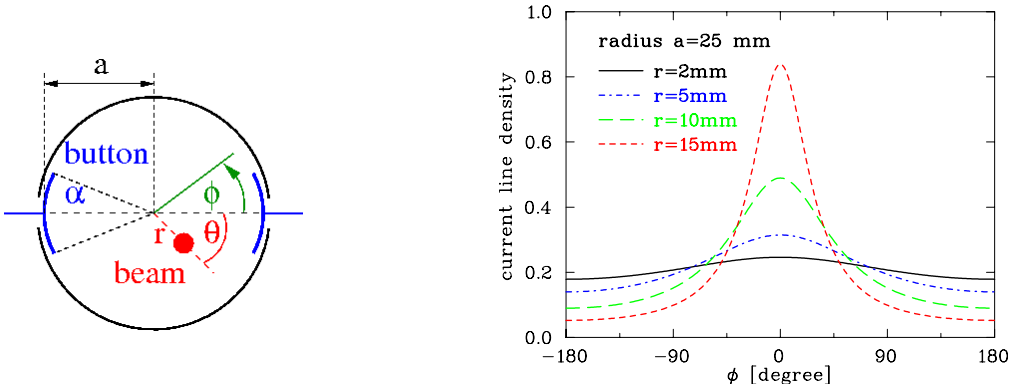

Fig. 19: Schematics for a button BPM and the image current density generated by a 'pencil' beam at different displacements r for an azimuth $\theta = 0$.

density j_{im} at the beam pipe of radius a is given as a function of the azimuthal angle ϕ as

$$j_{im}(\phi) = \frac{I_{beam}}{2\pi a} \cdot \left(\frac{a^2 - r^2}{a^2 + r^2 - 2ar \cdot \cos(\phi - \theta)} \right) \tag{19}$$

and is depicted in Fig. 19; see [16] for a derivation. As discussed above in Chapter 2.3, this represents the proximity effect, where the current density depends on the distance with respect to the beam center. The buttons covering an angle α and the image current I_{im} is recorded as given by:

$$I_{im} = \int_{-\alpha/2}^{+\alpha/2} a \cdot j_{im}(\phi) d\phi \quad . \tag{20}$$

The resulting signal difference for opposite plates as a function of horizontal beam displacement shows a significant non-linear behavior as displayed in Fig. 20. This is improved by the normalization to the sum voltage yielding a better linearity up to about half of the pipe radius a. However, this is inferior

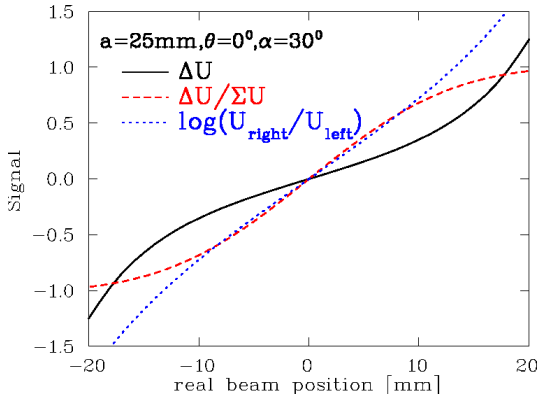

Fig. 20: Difference voltage, normalized difference and logarithmic ratio for a button BPM arrangement of angular coverage $\alpha = 30^o$ as a function of horizontal beam displacement i.e. $\theta = 0$ for a beam pipe radius $a = 25$ mm.

compared to the linear-cut BPMs. For this reason the linear-cut type is preferred as long as the relevant frequency range is sufficiently low as realized in most proton synchrotrons. An improved linearity can be achieved by logarithmic amplification of the individual plate signals, the electronic setup for this purpose is discussed in Chapter 7.3.

The non-linearity increases if the beam center moves outside the horizontal axis, which is depicted in Fig. 21 for different values of the azimuthal orientation θ as a function of horizontal displacement according to Eqs. 19 and 20. For an orientation along the diagonal line, a significant deviation from linearity starts for this case even at about 1/4 of the beam pipe radius. However, in the central part the reading is nearly independent of the orientation leading to a universal position sensitivity S. For the given case the value is $S = 7.4$ %/mm, which is larger than for an ideal linear-cut BPM having $S = 1/a = 4$ %/mm. The dependence between the horizontal and vertical plane is better depicted in the position map of Fig. 21, right: Here the real beam positions with equidistant steps are plotted as well as the results using $1/S \cdot \Delta U/\Sigma U$ calculations with S fitted at the central part. For the installations of these BPMs at Linacs, only the central, linear part is of interest for most applications and the position reading can be used directly. If a better accuracy is required, the reading after digitalization has to be corrected numerically, in most cases polynomial fits are chosen. Not only a single direction has to be considered, but due to the horizontal x and vertical y coupling mixed terms in the form $c_{nm} \cdot x^n y^m$ occur for the fit parameters c_{nm} using the signals from both planes.

In the discussion above a 'pencil' beam was considered having a beam radius much smaller than

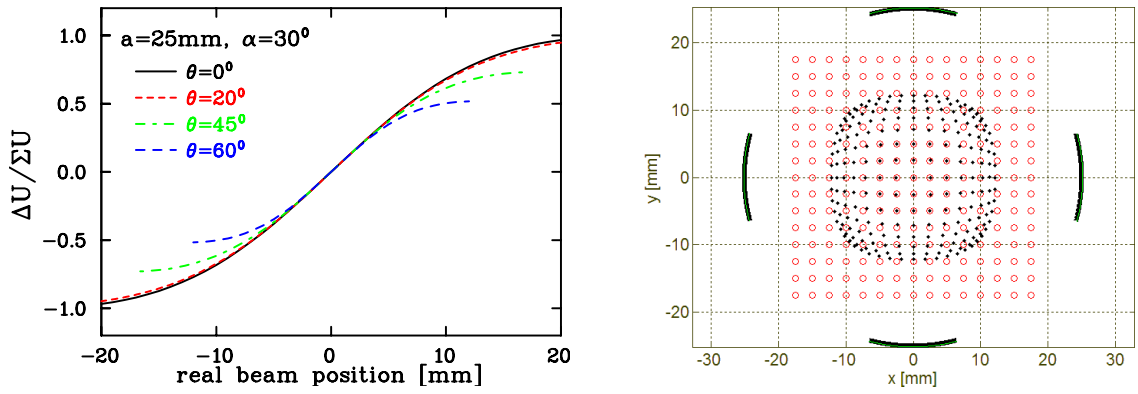

Fig. 21: Left: Horizontal position calculation for different azimuthal beam orientation θ for the parameters of Fig. 20. Right: In the position map the open circles represent the real beam position and the dots are the results of the $1/S \cdot \Delta U/\Sigma U$ algorithm with $S = 7.4$ %/mm for the central part.

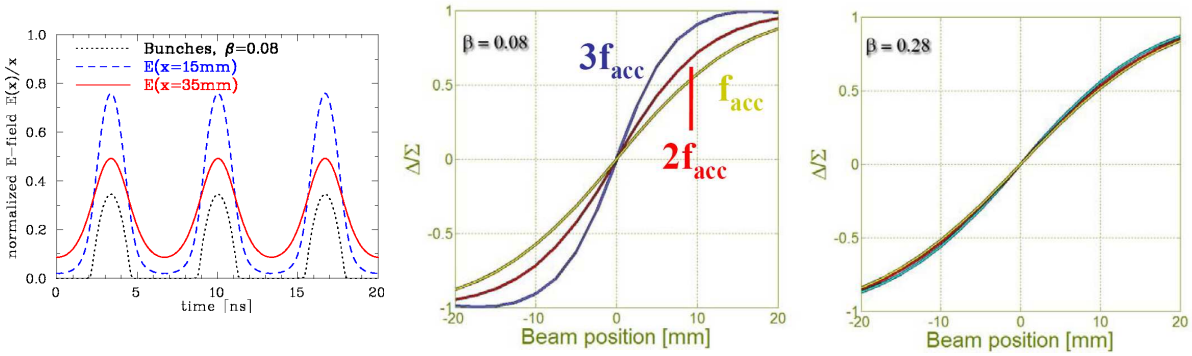

Fig. 22: Left: Transverse, normalized electric field at a distance of 15 mm and 35 mm between the BPM plates and bunches with $f_{acc} = 150$ MHz. Center: Position calculation for a beam of $\beta = 0.08$ at the fundamental frequency and its harmonics as a function of horizontal displacement and zero vertical displacement. Right: Position calculation of the same case but with $\beta = 0.28$. Other parameters like in Fig. 20.

the beam pipe size. If the beam size is comparable to the beam pipe, the non-linearity of the button response leads to a misreading. Moreover, the effect depends on the azimuthal orientation due to the coupling between the horizontal and vertical plane. To estimate the misreading, the signal strength according to Eqs. 19 and 20 have to be calculated for different values of r and θ. The results have to be weighed obeying the beam's transversal distribution. The effect is relatively small for a beam close to the center. However, the measurement cannot be corrected easily because the actual beam size at the BPM location has to be determined by transverse profile diagnostics.

The 2-dimensional electrostatic model delivers satisfying results and only minor corrections are necessary for a circular geometry and relativistic beam velocities i.e. TEM-like field pattern. As given by the electrical 50 Ω coupling scheme, the relevant frequency components are below the BPM's cut-off frequency and the signal strength does not depend on the BPM capacitance as given in Eq. 11. In contradiction to linear-cut BPMs, the relatively large spacing between the buttons prevent from cross talk between the four buttons and therefore the difference signal is not decreased significantly.

If the beam is accelerated to a non-relativistic velocity $\beta \ll 1$ only, as for proton Linacs and cyclotrons, the electric field cannot be described by a TEM wave anymore. Instead, the field pattern has a significantly longitudinal extension because the electric field propagation is faster than the beam velocity. Moreover, this field pattern strongly depends strongly on the beam displacement for opposite BPM plates, as shown in Fig. 22, left. In this example the transverse electric field is plotted for a beam of $\beta = 0.08$ accelerated by $f_{acc} = 150$ MHz and two different distances between the beam center and BPM plates. As determined by the electric field propagation, the duration of the signal is longer than the bunch distribution and for an increasing distance to the wall the signal gets less modulated, what is schematically shown in Fig. 2 as well. Generally, a weaker modulation of a time varying signal corresponds in frequency domain to a decrease of high frequency components. The frequency dependence on the position sensitivity is demonstrated for a horizontal displacement variation in Fig. 22, center. For a velocity of $\beta = 0.08$ the difference over sum signal depends on the evaluating frequency, a higher frequency increases the position sensitivity $S(\omega)$ in the central region. This is related to the strong dependence of the higher frequency content on the distance to the wall. However, for a larger displacement the sensitivity (defined as the derivative of the depicted curve according to Eq. 16) decreases to nearly zero and the BPM does not give any usable output at higher harmonics of f_{acc}. This is related to the fact, that the electric field for a large distance to the wall is smoothed, i.e. the high frequency components nearly vanish. For the given example of $f_{acc} = 150$ MHz the effect gets weaker for velocities above $\beta = 0.28$ as depicted in Fig. 22, right. The boarder of significance depends not only on β but also on f_{acc}: The variation of sensitivity S is stronger and continues to higher velocities if the acceleration frequency is larger.

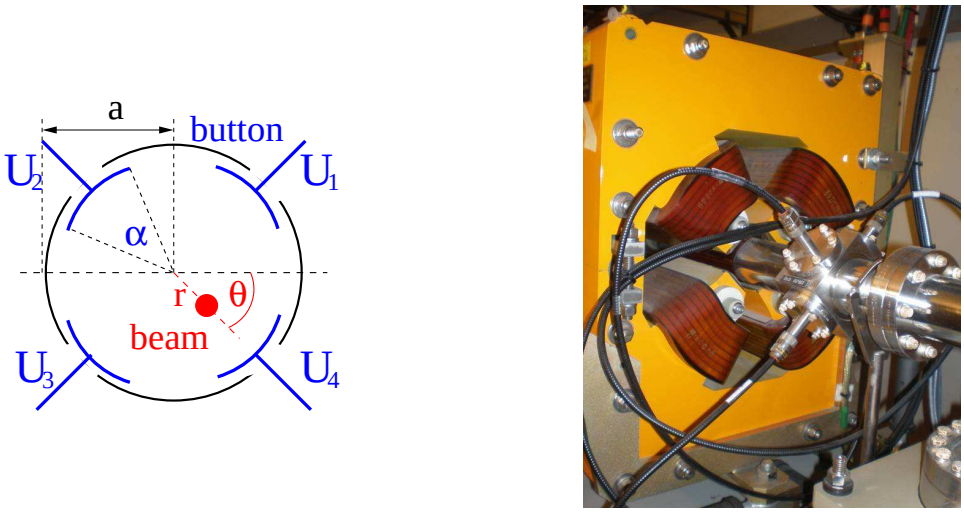

Fig. 23: Scheme of a rotated button BPM arrangement (left) and a photo of the realization mounted close to a quadrupole magnet at the ALS Booster-synchrotron , Berkeley (right).

The reason is the more severe modulation dependence for shorter bunches. A detailed discussion and an approximating formula can be found in [19], numerical calculations required for a realistic geometry are described in [20, 21].

At electron synchrotrons, the irradiation by synchrotron light mainly emitted in the horizontal plane can lead to radiation damage of the electrical insulator and the ceramic support of the button, leading to the risk of a BPM failure. At circular beam pipes the BPMs are therefore rotated by 45^o, as depicted in Fig. 23. The position reading in the horizontal and vertical plane is composed by a linear combination of all four button signals as

$$\text{horizontal: } x = \frac{1}{S} \cdot \frac{(U_1+U_4)-(U_2+U_3)}{U_1+U_2+U_3+U_4} \qquad \text{vertical: } y = \frac{1}{S} \cdot \frac{(U_1+U_2)-(U_3+U_4)}{U_1+U_2+U_3+U_4} \quad . \tag{21}$$

The range of linear behavior concerning the position sensitivity is reduced for this arrangement compared to the non-rotated orientation.

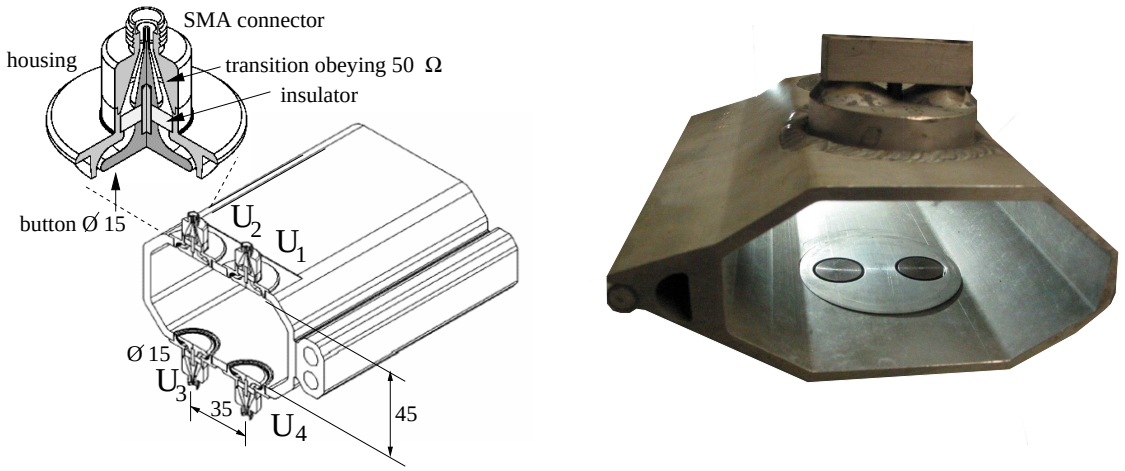

Fig. 24: Right: Typical button BPM arrangement within a vacuum chamber at a synchrotron light source, from [22]. Right: Photo of the realization at Hera.

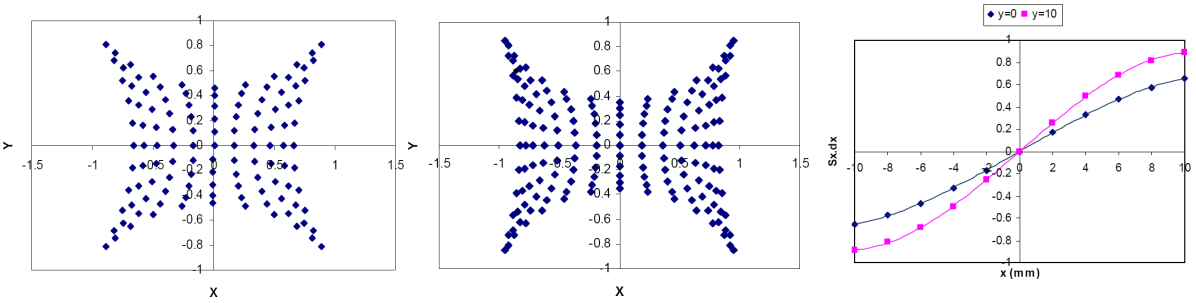

Fig. 25: Position map calculated with 2 mm displacement steps for the layout of planar oriented button BPMs of distance 24 mm (left) and 30 mm (middle); the units at the maps are cm. The height of the vacuum chamber is 30 mm. The sensitivity curve for a 24 mm button distance is shown right, from [24].

4.2 Planar arrangement of button BPM

Based on the quite different beam emittances in horizontal and vertical direction, the vacuum chamber does not have a circular shape at the storage rings of synchrotron light sources. Moreover, to avoid radiation damage in the plane of synchrotron light emission a planar BPM arrangement is required. A typical beam pipe shape and orientation of the BPMs is depicted in Fig. 24. The beam position is determined using the four button voltages according to Eq. 21 with different position sensitivities S_x and S_y in the orthogonal directions. Due to the more complex geometry a closed formula as Eq. 19 for the circular case does not exist and even for a 2-dimensional, electrostatic model numerical calculations are required, see e.g. [22, 23]. An instructive estimation from Ref. [24] is depicted in Fig. 25: The position map shows a large non-linearity and horizontal-vertical coupling. For a given beam pipe size and button diameter, the position sensitivity is influenced by the spacing between the buttons: As can be seen from the figure a larger distance leads to an improved resolution in the horizontal but a reduced separation in the vertical plane. The region of sufficient linearity is influenced by the button distance, as well. Compared to the circular geometry, the deviation from the linear behavior occurs for lower displacements as shown in Fig. 25 for the horizontal position calculation with two different vertical displacements. The values of the position sensitivity at the central part, in this example $S_x = 8.5$ %mm

Table 1: Simplified comparison between linear-cut and button BPM

	Linear-cut BPM	**Button BPM**
Precaution	bunches longer than BPM	bunches comparable to BPM
BPM length (typical)	10 to 20 cm per plane	Ø 0.5 to 5 cm
Shape	rectangular or cutted cylinder	orthogonal or planar orientation
Mechanical realization	complex	simple
Coupling	1 MΩ or $\sim$ 1 kΩ via transformer	50 Ω
Capacitance (typical)	30 - 100 pF	3 - 10 pF
Cut-off frequency (typical)	1 kHz for $R = 1$MΩ or 1 MHz for $R = 1$kΩ	0.3 to 3 GHz for $R = 50$Ω
Usable bandwidth (typical)	0.1 to 100 MHz	0.1 to 5 GHz
Linearity	very linear, no *x-y* coupling	non-linear, *x-y* coupling
Position sensitivity	good required: min. plate cross talk	good required: 50 Ω signal matching
Usage	at proton synchrotron, $f_{acc} < 10$ MHz	proton Linac, all electron acc. $f_{acc} > 100$ MHz

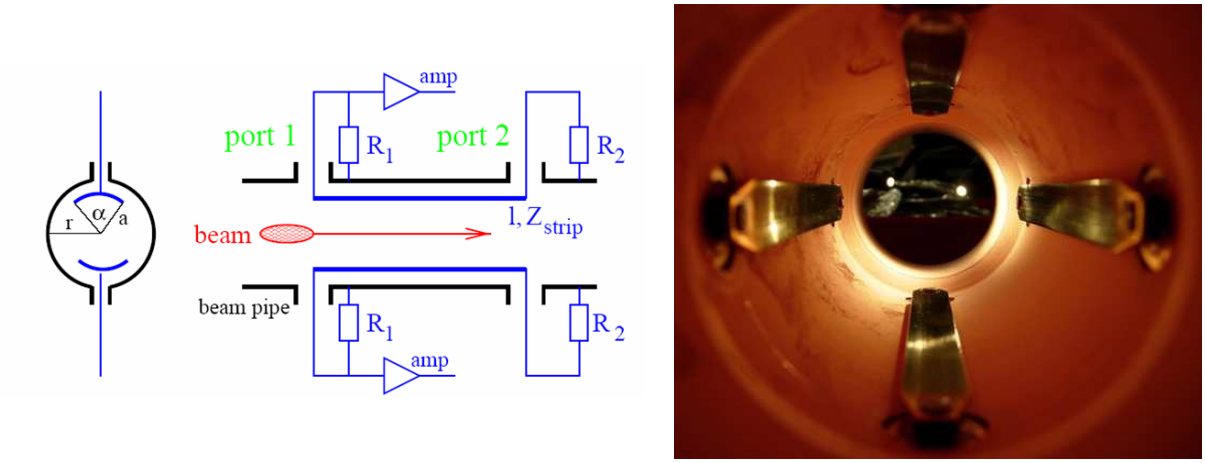

Fig. 26: Left: Scheme of a stripline pick-up. Right: Photo of the LHC stripline BPM of 12 cm length, from [18].

for $y = 0$ and $S_y = 5.6$ %/mm for $x = 0$, are comparable to the values one would obtain for the circular beam pipe. But in contrast to the circular arrangement, even at the central part the horizontal position sensitivity S_x depends on the vertical displacement y (and vice versa) and a correction algorithm using polynomial coefficients must be used for a precise position calculation.

As a summary the basic parameters for linear-cut and button BPMs are compared in Table 1. The table contains significant simplifications but should serve as an overview.

5 Stripline BPM

In the discussion of capacitive BPMs above, basically an electrostatic approach was used disregarding effects based on the signal propagation. If the bunch length becomes comparable to size the of the BPM, the final propagation time leads to a signal deformation, or in other words: For short bunches button BPMs have to be small and can therefore deliver only a low signal strength. Stripline BPMs are well suited for short bunch observation because the signal propagation is considered in the design like for transmission-lines in microwave engineering. The azimuthal coverage of the stripline BPM can be larger than of a button type yielding an increased signal strength. Moreover, stripline BPMs have the characteristic of a directional coupler which is of great importance for the installation in a collider of counter-propagating beams within the same beam pipe: With stripline BPMs one can distinguish between the directions of beam propagation and can record only the position from one beam by suppressing the signal from the counter-propagating beam, as explained below. The electrical properties of such a BPM are comparable to a directional coupler used for microwave devices [25].

A stripline pick-up consists of a transmission line of several cm length, having at both ends a feed-through with an impedance of R_1 and R_2 matched to 50 Ω, see Fig. 26. The stripline of length l is installed at a distance a from the beam center covering an angle of α within a cylindrical vacuum chamber of radius r. The characteristic impedance Z_{strip} of this strip depends on the parameters r, a and α, like for a micro-strip line on a printed-circuit board. It is chosen to be $Z_{strip} = 50\ \Omega$ for matching the characteristic impedance at the two ports, i.e. the condition $Z_{strip} = R_1 = R_2 = 50\ \Omega$ is fulfilled. Further on, we assume that the beam is relativistic and can be approximated by a traveling TEM wave with velocity v_{beam}, which equals the signal propagation on the strip $c_{strip} = v_{beam} = c$. The bunch length should be shorter than the strip length to prevent signal overlapping. The signal generation at the upstream port 1 during the bunch passage is visualized in Fig. 27 and described in the following:

– At $t = 0$ the bunch passes the front edge of the strip. The wall current is divided in two parts due to the matching of the voltage divider $Z_{strip} = R_1 = 50\ \Omega$. Half of this signal travels towards port 1 and half travels downstream along the stripline.

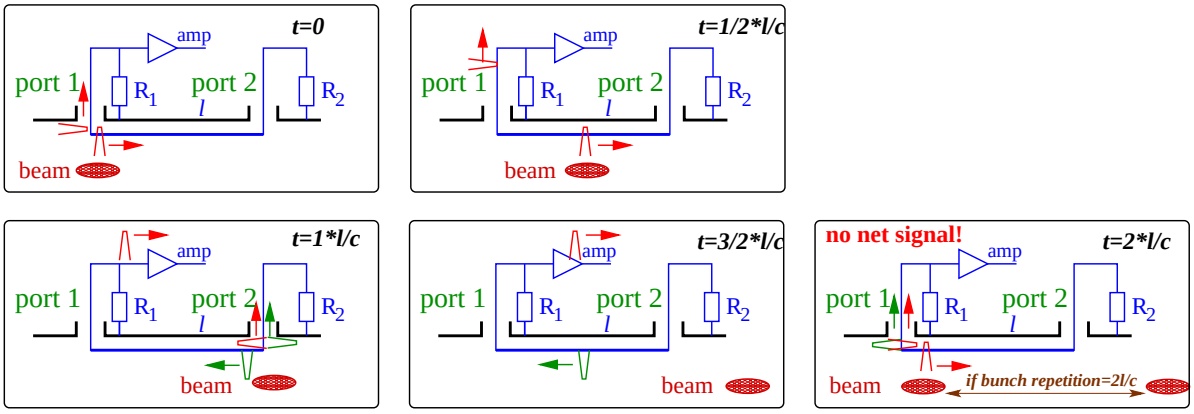

Fig. 27: Four plots visualize the signal generation at a stripline BPM. The plot on the lower right shows the signal cancellation in case of a bunch repetition by $t = 2l/c$.

- During $0 < t < l/c$ the beam and the signal travel in phase according to the condition $c_{strip} = v_{beam} = c$.
- At $t = l/c$ the bunch reaches the upstream port 2. Here the image charge leaves the stripline, generating an equal amplitude but opposite sign of current which is split in two halves according to $Z_{strip} = R_2 = 50\ \Omega$. However, the image current is leaving the detector and has the opposite sign to that generated at the upstream port. Therefore, half of the signal cancels the initially generated signal at port 1. The other half travels now back towards the upstream port 1.
- At time $t = 2 \cdot l/c$ the back traveling signal generated at port 2 reaches the upstream port 1.
- If the bunch repetition time of the bunches is $t_{acc} = 2 \cdot l/c$ the reflected, inverted signal from the first bunch cancels the signal from this second bunch.

This ideal behavior has two important consequences: Firstly, there is no signal at the upstream port 2 for a beam propagating in the described direction. For a second beam traveling in opposite direction, the roles of the ports are interchanged, which enables the separation of signal from counter-propagating beams like in colliders; this is not possible for other types of BPMs. However, due to imperfections of the mechanical and electrical realization, the suppression of the counter-propagating signals (i.e. signal strength at port 2 compared to strength at port 1) is typically 20 to 30 dB, i.e. the voltage at port 2 is lower by a factor 10 to 30. Secondly, the voltage signal for the ideal case at port 1 is given by

$$U_1(t) = \frac{1}{2} \cdot \frac{\alpha}{2\pi} \cdot R_1 \left(I_{beam}(t) - I_{beam}(t - 2l/c) \right) \quad . \tag{22}$$

Inserting a Gaussian bunch distribution as $I_{beam}(t) = I_0 \cdot \exp(-t^2/2\sigma_t^2)$ this equation can be written as

$$U_1(t) = \frac{Z_{strip}}{2} \cdot \frac{\alpha}{2\pi} \left(e^{-t^2/2\sigma_t^2} - e^{-(t-2l/c)^2/2\sigma_t^2)} \right) \cdot I_0 \quad . \tag{23}$$

This voltage signal at port 1 is shown in Fig. 28 for several bunch durations σ_t.

The related transfer impedance Z_t is obtained from the Fourier transformation of such a stripline BPM to be

$$Z_t(\omega) = Z_{strip} \cdot \frac{\alpha}{4\pi} \cdot e^{-\omega^2\sigma_t^2/2} \cdot \sin(\omega l/c) \cdot e^{i(\pi/2 - \omega l/c)} \tag{24}$$

and is shown in Fig. 28. For a short bunch it shows the following features:

- $|Z_t|$ is composed of a series of maxima for $f_{max} = \frac{c}{4l} \cdot (2n-1)$ for $n = 1, 2, ...$
- For a given acceleration frequency f_{acc}, the length l must be chosen to work close to such a maximum. The first maximum is located at $l = \frac{c}{4 f_{acc}} = \lambda/4$, with λ being the 'wave length' of the bunch repetition. Due to this behavior such BPMs are called quarter wave couplers.

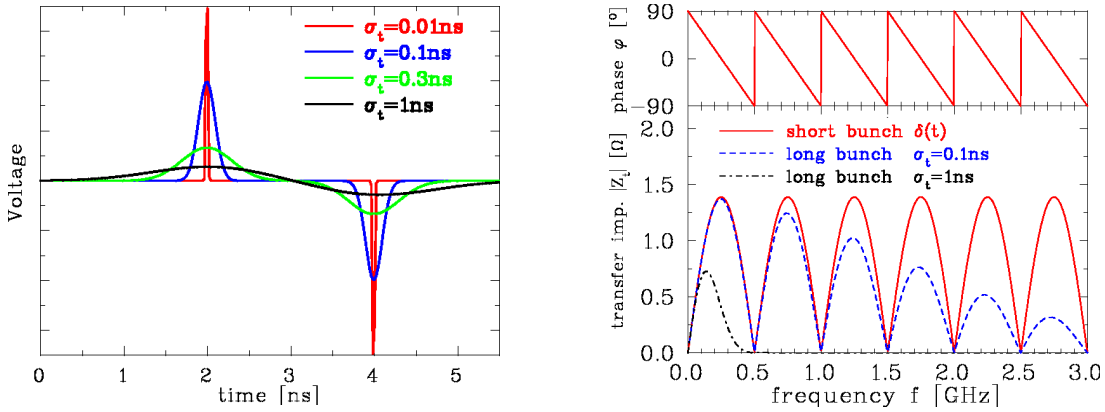

Fig. 28: Calculation of a voltage signal at the upstream port of a stripline BPM of $l = 30$ cm and a coverage of $\alpha = 10^o$ for different bunch durations σ_t (left) and the corresponding transfer impedance (right).

- The sensitivity is zero for $l = n \cdot \lambda/2$. This means no signal is present when the spacing between bunches is equal to $2l$ due to the destructive interference between consecutive bunches.
- The phase φ as a function of frequency is built of straight lines with a zero phase shift at the maxima locations for $l = (2n-1)/4 \cdot \lambda/4$. For these frequencies, the recorded signal is a direct image of the bunch. In contrast to capacitive pick-ups, short bunches can be monitored without signal deformation close to these frequency locations.

For a finite bunch duration σ_t, the transfer impedance decreases for increasing frequency as given by the term $|Z_t| \propto e^{-\omega^2\sigma_t^2/2}$ in Eq. 24. This is related to the fact, that the overlap of direct and reflected signal leads to a destructive interference. For a bunch length comparable to the stripline length, even the first maximum of the transfer impedance can be effected. However, in most cases the length of the stripline can be chosen with the objective of avoiding signal damping.

The position sensitivity of the four strips of such BPM can be calculated in the same way as for button types, see Eq. 19 and 20. In case of low beam current the azimuthal coverage α can be enlarged to intercept more image current leading to an increased signal amplitude without too much signal distortion. However, the characteristic impedance of the strips has to be kept to $Z_{strip} = 50\ \Omega$

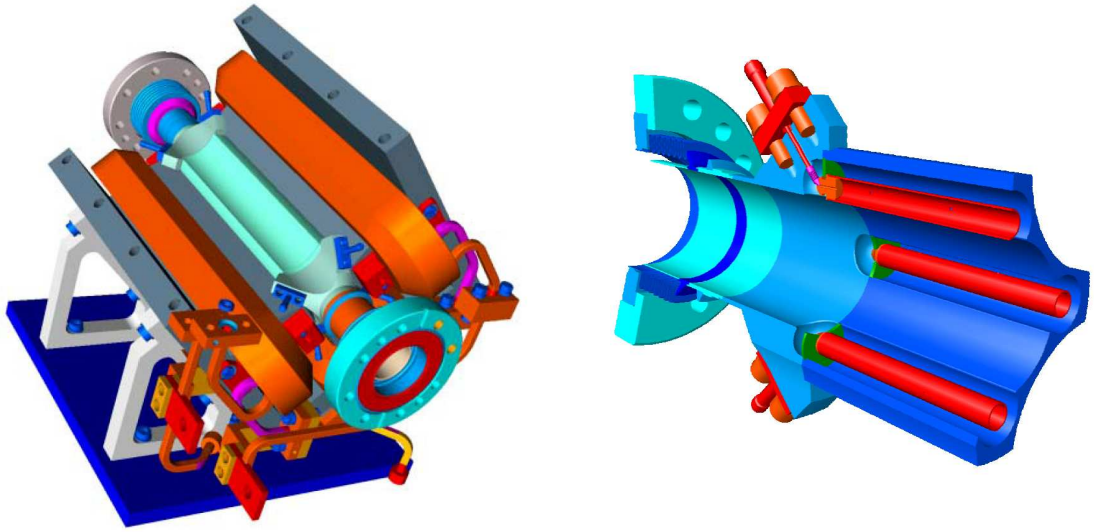

Fig. 29: Technical drawing of the stripline BPM installed inside a quadrupole magnet at TTF2 (left) and the design of the transition for the strip to the feed-through (right). The beam pipe has Ø 34 mm, from [26, 27].

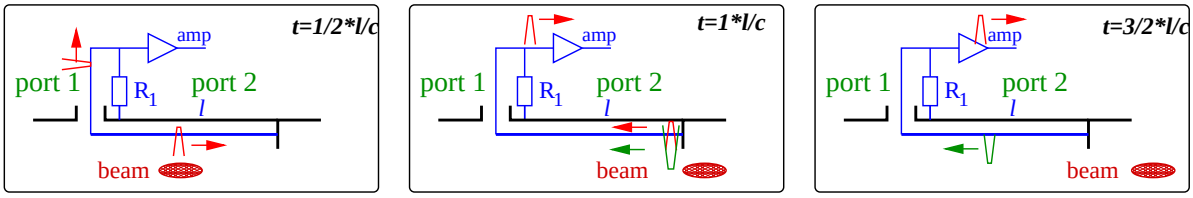

Fig. 30: Schematic for the signal generation at shorted stripline BPM.

resulting in an increased mechanical size of the beam pipe. Moreover, the signal propagation towards the feed-through have to fulfill this matching condition. Even for smaller azimuthal coverage, the electrical transition for the strips to the coaxial vacuum feed-through has to be designed carefully obeying sensitive radio-frequency and mechanical requirements. The realization of a stripline BPM is more complex compared to the button type. An example of the technical design [26] for the electron Linac at TTF2 is shown in Fig. 29. The striplines can be installed inside a quadrupole magnet reducing the insertion length for the BPM installation.

The so called shorted stripline BPM is a modification in a way, that the downstream port is replaced by a short circuit leading to a facile and more compact mechanical installation; for a realization see e.g. [28, 29]. The consequence of this modification is explained according to Fig. 30: The signal traveling with the beam is reflected at end of the stripline, but due to the short circuit of $R = 0$ at this location the polarity remains. It is added to the signal created by the leaving bunch having the reversed polarity and twofold amplitude compared to the co-propagating signal. The result is a counter-propagating signal with the original signal strength but reversed polarity i.e. the same signal shape as for regular stripline BPMs is finally recorded at the upstream port.

Shorted stripline BPMs are used at proton Linacs for beams with non-relativistic velocities with a kinetic energy below 1 GeV [30, 31, 32]. In this case the beam velocity $v_{beam} < c$ is lower than the signal propagation velocity and Eq. 23 has to be rewritten as

$$U_1(t) = \frac{Z_{strip}}{2} \cdot \frac{\alpha}{2\pi} \left(e^{-t^2/2\sigma^2} - e^{-(t-l\cdot\zeta)^2/2\sigma^2} \right) \cdot I_0 \quad \text{with} \quad \zeta = (1/c + 1/v_{beam}) \ . \tag{25}$$

Table 2: Simplified comparison between stripline and button BPM

	Stripline BPM	**Button BPM**
Idea for design	traveling wave	electro-static
BPM size (typical)	length: 5 to 30 cm per plane transverse coverage up to $\alpha \simeq 70^0$	Ø 0.5 to 5 cm otherwise signal deformation
Signal quality	minor deformation	possible defromations due to finite size and capacitance
Signal strength	larger depending on trans. coverage	smaller
Bandwidth	nearly broadband with well defined minima	highpass with $f_{cut} \simeq 3$ GHz
Requirement	careful 50 Ω matching	
Mechanical realization	complex	simple
Installation	inside quadrupole possible	compact due Ø < 3 cm
Directivity	**yes**	no

The amplitude of the transfer impedance is modified as

$$|Z_t(\omega)| = Z_{strip} \cdot \frac{\alpha}{4\pi} \cdot e^{-\omega^2\sigma_t^2/2} \cdot \sin\left[\frac{\omega l}{2} \cdot \left(\frac{1}{c} + \frac{1}{v_{beam}}\right)\right] \tag{26}$$

The transfer impedance not only depends on the bunch duration but also on the beam's velocity. Along a Linac the optimal length of the BPM for maximal signal strength would increase as can be calculated from the first maximum of the transfer impedance. This maximum fulfills the condition $\frac{\omega l}{2} \cdot (\frac{1}{c} + \frac{1}{v_{beam}}) = \frac{\pi}{2} \Rightarrow l_{opt} = 1/2 \cdot v_{beam}/f_{acc}$. Nevertheless, in most installations the BPM have a constant length to simplify the mechanical construction and signal deformations are accepted. A compact assembly within the quadrupole magnets is sometimes realized. A typical length is less than 5 cm with a relatively large azimuthal coverage of $\alpha \simeq 60^o$ for high signal amplitudes.

The basics of stripline BPMs are summarized in Table 2 and compared to the button type. Due to the precise matching condition required for the stripline type, the technical realization is complex. Beside the possibly larger signal strength and bandwidth, the main advantage of stripline BPMs is their directivity which is necessary at any collider with counter-propagating beams in a common beam pipe.

6 Further types of BPM

Within this chapter we briefly introduce three further types of BPMs. The wall current monitor types are based on a resistive or inductive broadband detection of the wall current and allow for longitudinal bunch structure observation. In a cavity BPM a resonator mode is excited with an amplitude proportional to the displacement. Tiny displacements of $x < 1\ \mu$m for beam pulses as short as $1\ \mu$s can be detected. This is an important requirement for short-pulses delivered by free electron lasers or at electron-positron-collider projects. Even more types of BPMs have been realized but cannot be discussed here, like capacitive types with an external resonator to improve the low signal detection threshold, inductive types based on the beam's magnetic field measurement [33, 34, 35] or traveling wave structures well suited for observation above several GHz [36, 37, 38].

6.1 Resistive wall current monitor

The evolution of the bunches along an accelerator or within a synchrotron is influenced by the longitudinal emittance and therefore a bunch structure observation is of great interest. It is advantageous to have an equalized transfer impedance $Z_t(f)$ as a function frequency, i.e. the large bandwidth leads to a non-modified image of the beam bunches. In a synchrotron the evolution of the bunches can be observed and analyzed e.g.[39, 40], while for electron beams the observation of short bunches is of importance [41, 42].

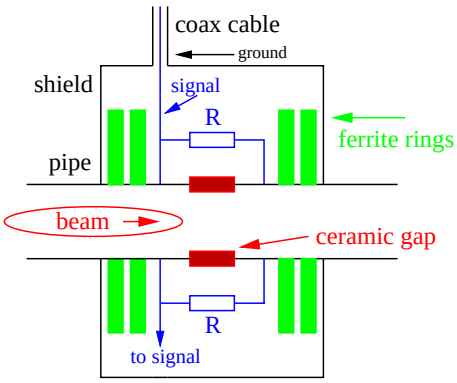

Fig. 31: Scheme of a wall current monitor.

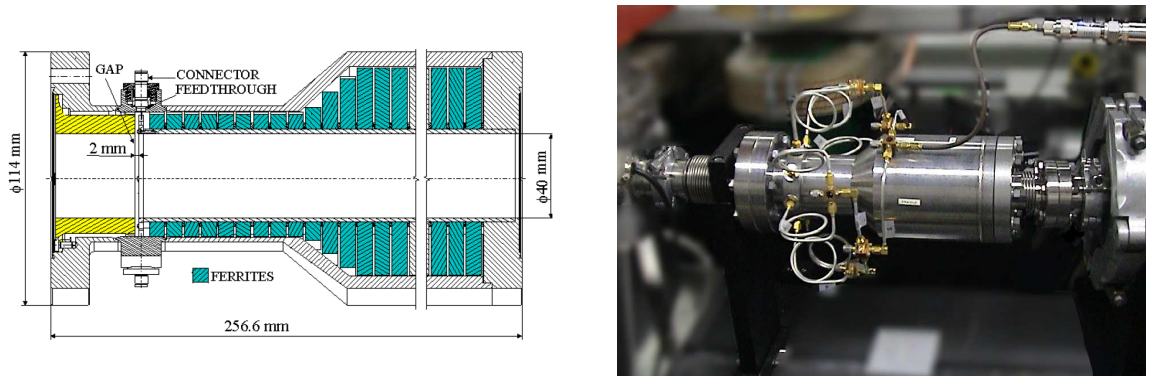

Fig. 32: The realization of a wall current monitor at a Ø 40 mm beam pipe for CTF, from [41].

With a resistive **W**all **C**urrent **M**onitor **WCM**, a bandwidth with a lower cut-off frequency down to kHz and an upper value up to several GHz can be realized. The image current flowing along the beam pipe is interrupted by a ceramic gap shorter than the bunch length, as displayed schematically in Fig. 31. The gap is bridged by typically n =10 to 100 resistors with a low resistivity of R =10 to 100 Ω leading to a total value of $R_{tot} = R/n \sim 1\ \Omega$. The voltage drop at the resistors is the signal source; these resistors are azimuthally distributed in an equal manner, so that the signal amplitude is independent of the actual beam position. At several locations the signal is connected to a coaxial cable and fed to an amplifier. Within the passband the voltage across the resistors U_{tot} is given by $U_{tot} = \frac{R}{n} \cdot I_{beam}$.

The resistors have to be shielded carefully against noise from the surroundings as caused, e.g. by ground currents from the rf-system. The shield also acts as a short circuit for low frequencies. To achieve a low cutoff frequency, high-permeable ferrite rings are mounted across the beam pipe to force the image current through the resistors. The equivalent circuit of such a WCM is a parallel shunt of the capacitance C of the ceramic gap, the resistors R_{tot} where the voltage is measured and the inductance L as given by the ferrites. The transfer impedance and its frequency response can be calculated from $Z_t^{-1} = R_{tot}^{-1} + i\omega L^{-1} + i\omega C$. For the ideal case, the lower cut-off frequency is $f_{low} = 2\pi \cdot R_{tot}/L$ and can be decreased down to $f_{cut} \sim 10$ kHz. The upper cut-off frequency is given by the capacitance of the gap to be $f_{high} = (2\pi \cdot R_{tot} \cdot C)^{-1}$; several GHz are realizable by a careful design of all rf-components. Within this bandwidth the transfer impedance is $|Z_t| = R_{tot}$ and $\varphi = 0^o$ allowing un-differentiated bunch structure observation. The realization for CTF shown in Fig. 32 has a bandwidth over 6 decades from 10 kHz to 10 GHz, for more details see [41]. Other realizations are described e.g. in [40, 43]. The device is rarely used for beam position determination.

6.2 Inductive wall current monitor

For position determination the wall current monitor principle is modified to sense directly the azimuthal image current distribution by at least four strips and is called inductive WCM. The beam pipe is intersected by a ceramic gap and the current strips are installed outside of the beam pipe for better accessibility, see Fig. 33. The wall current is sensed by a transformer surrounding each strip i.e. each strip acts as the primary winding of this transformer. The transformer's secondary winding of about 10 to 30 turns is fed to an amplifier for further analog processing. As for the resistive counterpart, ferrites are used to force the low frequency components to the current strips. A realization is described in [44] and depicted in Fig. 33. It uses 8 current strips mounted at a radius of Ø 145 mm around the Ø 120 mm beam pipe. The reached position sensitivity for this device is $S = 3.8$ %/mm which is about a factor of 2 larger than an ideal linear-cut BPM. The linearity in the central part of ±20 mm is very high with less that 0.1 mm deviation, as shown in Fig. 34. A large bandwidth with flat frequency response over 6 orders of magnitude is achieved. The large bandwidth and the fact that all sensitive parts are installed outside of the vacuum are the main advantages of this BPM type.

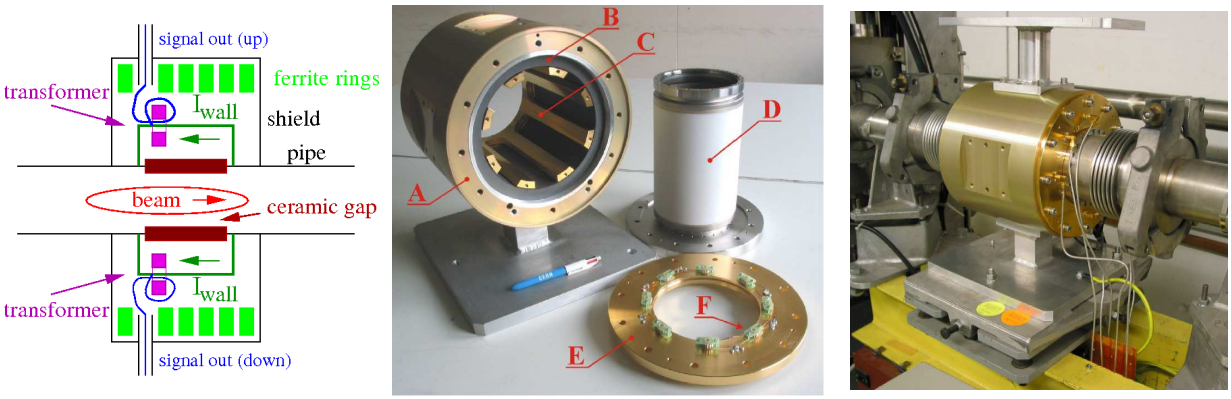

Fig. 33: Scheme of an inductive wall current monitor and the realization for CERN LINAC 2, from [44]. The abbreviations at the central photo are: A housing, B ferrite rings, C current strips on Ø 145 mm, D ceramic gap of Ø 120 mm, E support and F current transformers for the 8 strips.

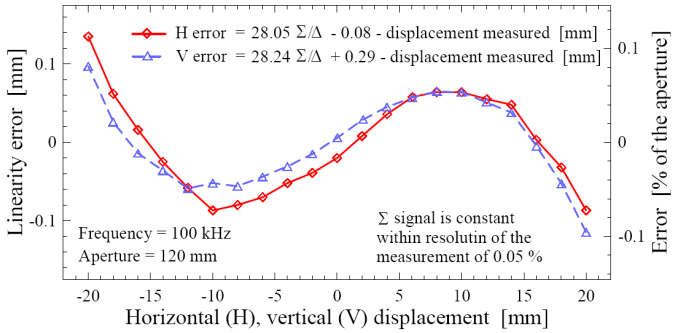

Fig. 34: Linearity determination in the central region of the inductive WCM of Fig. 33, from [44].

6.3 Cavity BPM

Precise beam alignment is required for Linac-based electron-positron colliders and free electron lasers due to their high demands on accuracy and the very small beam sizes. Moreover, only short pulses of less than 1 μs duration are accelerated with low repetition rate, calling for single pulse measurements without averaging possibilities. A resolution requirement is typically 1 μm for a single pulse of 1 μs duration. These challenges can be approached by the excitation of resonator modes within a cavity BPM. Because the short bunches deliver a wide spectrum of frequencies several modes resonating at slightly different frequencies can be excited. Due to the resonating behavior the position sensitivity, as given by the shunt impedance of the dipole mode (see below), is higher than for a button or stripline BPM. The subject is reviewed in [45] and only the basic idea for a pillbox structure is presented here.

In a pillbox cavity the wavelength of the resonator mode is fixed by the cavity size due to the boundary conditions for the electric field at the metallic walls. The field pattern of the monopole mode within a circular pillbox cavity is shown in Fig. 35. It has a maximum of the electric field in the center of the cavity and is excited proportional to the bunch charge. This mode has a field patter of TM_{010} characteristics [46, 47] with the resonator frequency f_{010}; it is sometimes called common mode, too. For typical cavity sizes of 5 to 15 cm the resonance frequency is in the order of several GHz. The dipole mode has a node at the cavity center as described by the TM_{110} field pattern and a resonator frequency f_{110} which is separated from the monopole mode frequency by several 100 MHz. Its excitation amplitude depends linearly on the beam displacement (as well as on the bunch charge). The amplitude of the resonating TM_{110} field and its phase has to be processed, the magnitude represents the value of the beam displacement and the sign is reconstructed from the phase. The phase is defined relative to the phase of the monopole mode, which has to be processed in addition. The horizontal and vertical displacements

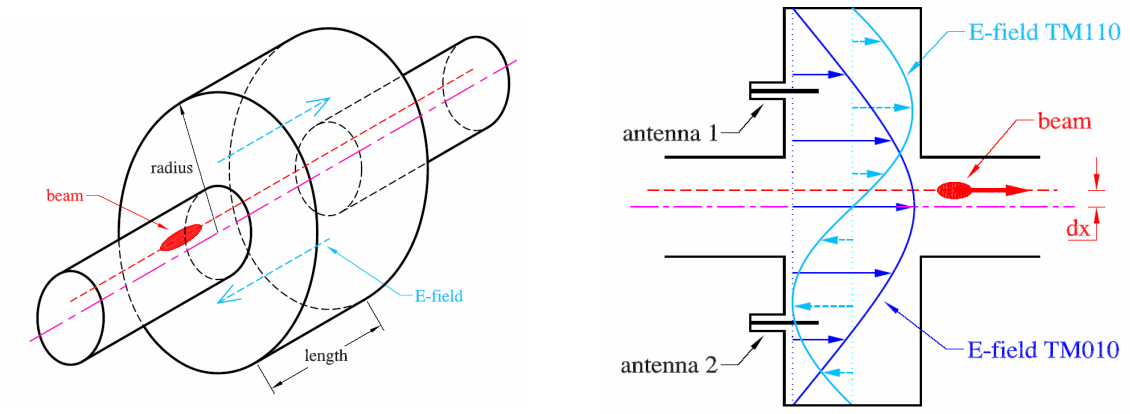

Fig. 35: Left: Scheme of a cavity BPM in pillbox geometry. Right: Schematic electric field distribution of the monopole (TM_{010}) and dipole mode (TM_{110}).

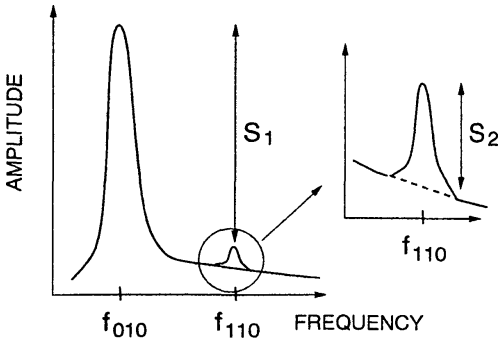

Fig. 36: Schematic frequency spectrum of a pillbox cavity.

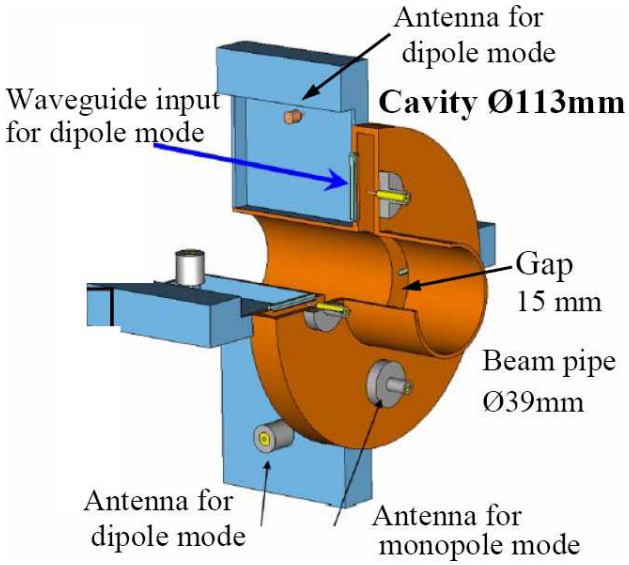

Fig. 37: Layout of a cavity BPM designed at FNAL [48].

can be distinguished by the different polarization of the two possible dipole modes. The loaded quality factor Q_{load} for both modes is chosen to be typically 100 to 1000. A larger value gives a higher signal strength, but reduces the time resolution and by that the possibility to resolve consecutive pulses of about μs repetition time.

For typical displacements of several μm only the dipole mode is excited weakly, while the monopole mode with the maximal electric field on axis is excited efficiently. Due to the relatively low quality factor, the frequency spectrum is wide and a noticeable amount of the power from the monopole mode is present at the frequency of the dipole mode, as depicted schematically in Fig. 36. An effective method must be chosen to separate the weak dipole mode signal from the monopole contamination.

An example of such a device is shown in Fig. 37 as designed at FNAL for the International Linear Collider [48, 49]. The diameter of the cavity is Ø 113 mm interrupting the Ø 39 mm beam pipe by a gap of 15 mm length. The loaded quality factor is $Q_{load} \simeq 600$. The resonance frequencies of $f_{010} = 1.125$ GHz and $f_{110} = 1.468$ GHz are relatively low. The antennas for the coupling to the monopole mode are

short N-type feed-through. The signal for the dipole mode is coupled out via a waveguide at a position of large electric field amplitude. It has its cutoff frequency above the f_{010} resonance to suppress the propagation of the monopole mode toward the antennas for the dipole mode detection. A resolution on a single pulse basis of < 1 μm for a displacement range of ± 1 mm has been achieved. Examples of other recent realizations and descriptions of the principle can be found in [50, 51].

7 Electronics for signal processing

7.1 General considerations

The electronic circuit attached to the BPM plates influences the properties of the signal shape and is therefore an important part of the full installation. By the choice of the analog and acquisition bandwidth, the time steps for meaningful data presentation is determined and this has to be matched to the foreseen measurements and applications. A wide range is covered by BPM systems: The highest bandwidth is required, if the structure of the individual bunches has to be observed; for this case the bandwidth has to exceed the acceleration frequency by typically a factor of 10. For a bunch-by-bunch observation the signal from individual bunches has to be distinguishable i.e. the bandwidth has to be at least comparable to the acceleration frequency. For such a mode, each bunch delivers a position value and they are used to monitor the dynamic behavior during acceleration or to determine lattice parameters. For the turn-by-turn mode at a synchrotron, the position information of a dedicated bunch on each turn is stored and lattice parameters like the tune are calculated. The required analog bandwidth is chosen to separate one dedicated bunch from the successive bunches. At most synchrotrons the circulating beam is composed of many (10 to several 100) bunches and therefore the acquisition bandwidth can be lower than the analog bandwidth and is typically about some MHz. A much lower bandwidth is required for monitoring slow beam variations with high resolution, like the closed orbit within a synchrotron, where the averaged behavior during thousands of turns is determined. The discussed choice of processing bandwidth significantly influences the position resolution from about 100 μm or 10^{-3} of beam pipe diameter for the single bunch reading down to typically 1 μm or 10^{-5} of beam pipe diameter for a closed orbit measurement with less than 1 kHz bandwidth. Beside the technical demands, the cost of the BPM electronics is a design criterion with regard to the large amount of BPM locations around the accelerator.

For the low difference signal of opposite BPM plates, the thermal noise gives a general limitation on the achievable position resolution δx. For the difference of sum evaluation it is

$$\delta x = \frac{1}{S} \cdot \frac{U_{eff}}{\Sigma U} \quad . \tag{27}$$

The thermal noise is described by an effective voltage drop U_{eff} at a resistor R as given by

$$U_{eff} = \sqrt{4 k_B \cdot T \cdot R \cdot \Delta f} \tag{28}$$

with k_B the Boltzmann constant, T the temperature of the resistor R and Δf the bandwidth of the analog or digital processing. A lower bandwidth results in a lower thermal noise contribution, corresponding to an increased position resolution. This is depicted in Fig. 38 where the measured position resolution is plotted for three different bandwidth settings of the same readout chain [52]; in Chapter 7.6 the appropriate electronics is discussed. A bandwidth restriction from 500 kHz (for the turn-by-turn mode) to 2 kHz (for the closed orbit mode) leads to a better resolution of about $\sqrt{2\text{ kHz}/500\text{ kHz}} \simeq 1/15$ as expected from Eq. 28. This reduction is true for a large signal amplitude, corresponding a large beam current. For lower input signals, the relative contribution of the constant thermal noise rises, resulting in a worse signal-to-noise ratio and therefore a lower position resolution; in the displayed example by two orders of magnitude for a current decrease by a factor of 100. Note that an input level of -80 dBm corresponds to a voltage of 30 μV at 50 Ω only. Moreover, the signal has to be amplified and additional noise from the amplifier input stage (as characterized by its noise figure F) is added. Further signal perturbations might be caused by electro-magnetic pick-up from the surrounding environment which is most severe for weak

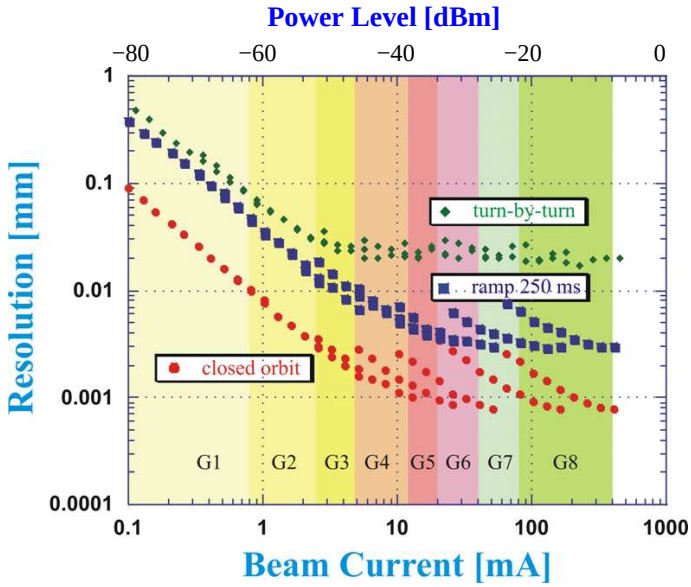

Fig. 38: Determination of the position resolution as a function of input level and corresponding beam current performed at the Swiss Light Source for different bandwidths: 500 kHz (turn-by-turn mode), 15 kHz (here called ramp 250 ms mode) and 2 kHz (closed orbit mode). Gain levels of the system are kept constant for the marked beam current ranges (colored underlays G1 to G8), from [52, 53].

signals and therefore the first stage amplifier should be mounted close to the BPM. If low currents have to be monitored, a large signal strength is preferred, which corresponds to a large transfer impedance Z_t, realized in most cases by large BPM plates mounted as close as possible to the beam.

The analog electronic schemes can be divided in two categories, namely the broadband and narrowband processing. In the broadband case, the behavior of individual bunches can be monitored; the broadband processing with linear amplifiers and logarithmic-ratio processing belong to this category. For the narrowband case, the individual bunch properties are lost due to the bandwidth restriction. In modern installations the analog signal is digitized on an early stage and digital signal processing delivers the position information, offering flexible signal evaluation without any hardware modification. In Ref. [54] the various electronic schemes are compared.

7.2 Broadband linear processing

The most direct way of electronic treatment is the broadband processing shown in Fig. 39 which preserves the full information of the bunch structure and is required for a bunch-by-bunch evaluation. This scheme is mainly realized at proton synchrotrons due to the relatively low acceleration frequency and at proton Linacs to perform velocity measurements by monitoring the time-of-flight of a single bunch between two BPMs. The individual BPM plate signals are amplified with a broadband linear amplifier having a bandwidth up to about the 10-fold acceleration frequency. The impedance of the input stage can be chosen to be either high impedance, as sometimes used at proton synchrotrons having a bandwidth limitation to typically 100 MHz, or 50 Ω with an increased bandwidth up to several GHz. If a passive impedance matching by a transformer is required (as discussed for Fig. 10) it is inserted in front of the amplifier. Two examples of such treatments for a synchrotron and a Linac were depicted in Fig. 6 and 7. To achieve the required dynamic range, gain switching of the amplifier is foreseen for matching the signal amplitude to the required ADC input level. In some cases the signal from the BPM plates can be that large, that attenuation is required. To ensure exact position measurements, a precise test pulse injection (at periods where no beam is present) allows for the compensation of possible gain variation caused by thermal drifts. The signal is digitized by a fast ADC, in the optimal case with a sample rate

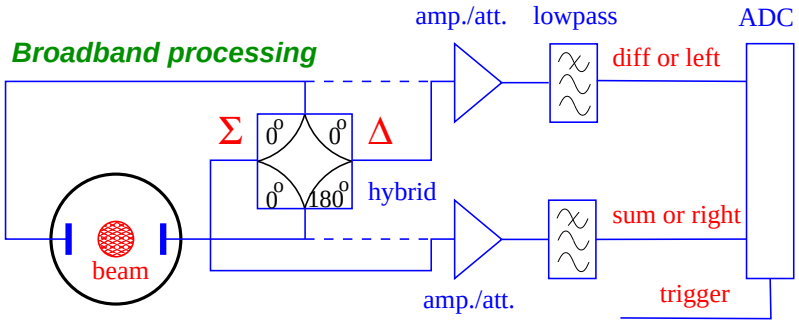

Fig. 39: Scheme of a broadband signal processing. The plate signals are either fed directly to the amplifier (dashed line) or via a hybrid the sum and difference is generated in an analog manner (solid line).

of 4 times the analog bandwidth. For noise reduction and alias-product suppression, a lowpass filter is used matched to the sample rate of the ADC. In older installations fast sampling was not possible and an external trigger, as generated from the bunch passage in an analog manner forced the digitalization. In most applications the sum and difference voltages are analogously generated by a 180^o hybrid or a differential transformer. Because they are pure passive devices, they can be mounted quite close to the BPM plates even in case of high radiation. The difference signal, which is normally lower by at least a factor of 10, can be amplified by a higher amount than the sum signal to exploit the full ADC range. An example of an amplifier design can be found in [55] and the usage of such a system in [56].

The advantage of the broadband realization is related to the fact that the full information is preserved and post-processing, in most cases in a digital manner, is possible, resulting in flexible high performance BPM readout. Linear amplifiers can cover a wide dynamic range by gain switching. This switching and the required high performance digitalization, i.e. an ADC with high sampling rate, leads to an extensive hardware realization. The disadvantage is the limited position resolution due to the broadband noise as well as the relatively extensive and costly hardware.

7.3 Logarithmic ratio processing

A very large dynamic range without gain switching can be achieved by using logarithmic amplifiers, see Fig. 40 for the schematics. A compression of the signal's dynamic range of up to 80 dB (corresponding to 4 orders of magnitude for the input voltage) is performed, where a ratio of input voltages corresponds to an output voltage difference. The related network within an integrated circuit consists of cascaded limiting amplifiers of several 100 MHz bandwidth [57, 58, 59]. Due to the intensive usage for telecommunication and broadcasting they are well developed and inexpensive. The output signal from the logarithmic amplifier is lowpass filtered for noise reduction. For most applications the lowpass cut-off frequency is typically MHz and individual bunches cannot be observed. But a higher cut-off frequency is also possible which is particularly useful for single bunch observation in transfer lines. The single plate signals are fed to a differential amplifier (based on low frequency operational amplifier technology) well suited for relatively low bandwidth processing. The output can finally be digitized by a slow sampling ADC.

The beam position for this electronic processing is

$$x = \frac{1}{S_x} \cdot \left(\log U_{right} - \log U_{left}\right) = \frac{1}{S_x} \cdot \log \frac{U_{right}}{U_{left}} \propto \frac{1}{S_x} \cdot U_{out} \tag{29}$$

with the position sensitivity given in $S_x = [\mathrm{dB/mm}]$ for the horizontal direction; for the vertical direction a corresponding formula can be applied. The output voltage U_{out} after the differential amplifier is independent of the sum voltage ΣU and therefore of the beam current. It is shown in Fig. 20 for button

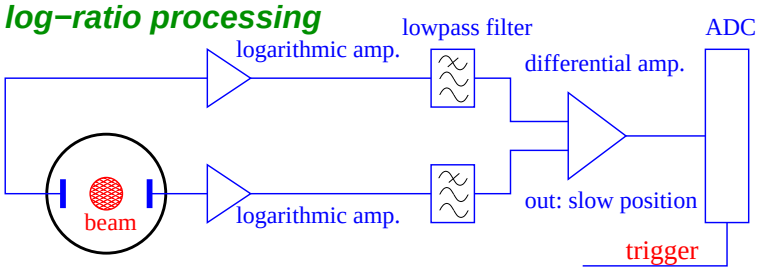

Fig. 40: Scheme of a logarithmic amplifier chain.

BPMs in a circular arrangement, that this type of processing leads to an improved linear position reading compared to the difference over sum $\Delta U/\Sigma U$ algorithm.

The advantage of logarithmic-ratio processing is the large dynamic range without gain switching, resulting in a robust and inexpensive electronics realization. In most cases a commercially available board is used [60]. The disadvantage is a relatively low temperature stability and output linearity as a function of input voltages, resulting in a poor position accuracy. Due to the differential amplifier the intensity information is lost.

7.4 Analog narrowband processing

For a long train of bunches delivered by a Linac or stored in a synchrotron, the signal recorded by the BPM has a repetitive behavior, which corresponds to a line spectrum in frequency domain as discussed in Chapter 2.2. A significant reduction of the broadband thermal noise is possible by analyzing the BPM signal at one harmonic of the acceleration frequency only. Bandpass filters with a narrow passband are not well suited for this purpose due to their ringing behavior. Instead, after passing a linear amplifier, a mixing stage is introduced as depicted in Fig. 41. This principle is called heterodyne mixing and is realized e.g. for a spectrum analyzer and even for any AM-radio. In this sense one can express the signal composition for position measurement in the following words: The position information is transmitted on carrier frequency and demodulation is required to extract the amplitude. A mixer is a passive rf-device multiplying a wave at the RF-port (for radio frequency) with one at the LO-port (for local oscillator). The product oscillates at the difference and sum frequency and is available at IF-port (for intermediate frequency). The LO-port is connected to a sine wave oscillating with the acceleration frequency shifted by a certain amount $U_{acc}(t) = \hat{U}_{acc} \cdot \cos \omega_{acc} t$. The RF-port is connected to the BPM voltage $U_{BPM}(t) = \hat{U}_{BPM} \cdot \cos \omega_{BPM} t$. From the trigonometric theorem $\cos a \cdot \cos b = 1/2 \cdot [\cos(a-b) + \cos(a+b)]$ it follows

$$U_{IF}(t) = \hat{U}_{acc} \cdot \hat{U}_{BPM} \cdot \cos \omega_{acc} t \cdot \cos \omega_{BPM} t = \frac{1}{2} \hat{U}_{acc} \cdot \hat{U}_{BPM} \cdot [\cos(\omega_{acc} - \omega_{BPM})t + \cos(\omega_{acc} + \omega_{BPM})t] \,. \tag{30}$$

The difference frequency content is available at the IF-port and is filtered by a narrow bandpass; typically 10.7 MHz or one of its harmonics is chosen due to its large usage in telecommunication. At a proton synchrotron an IF-frequency of about 100 kHz is chosen to perform down mixing with respect to the typical MHz acceleration frequency. The signal is rectified by a so-called synchronous detector to recover the amplitude content $\hat{U}_{IF}$. In a synchronous detector (depicted as part of Fig. 42) the signal is split and one branch is fed into a limiter amplifier driven into saturation, which transforms the signal to a bipolar rectangular pulse. This signal is mixed with the original signal to yield a unipolar waveform. It passes through a low-pass filter with a cut-off frequency well below the IF-frequency. The resulting quasi-dc level is then digitized by a slow ADC. The mixing and rectification is equivalent to an average over many bunches leading to high position resolution and good accuracy. Because the information for the individual bunches is lost, this method does not allow for a turn-by-turn observation. A realization of this scheme is described in [61, 62].

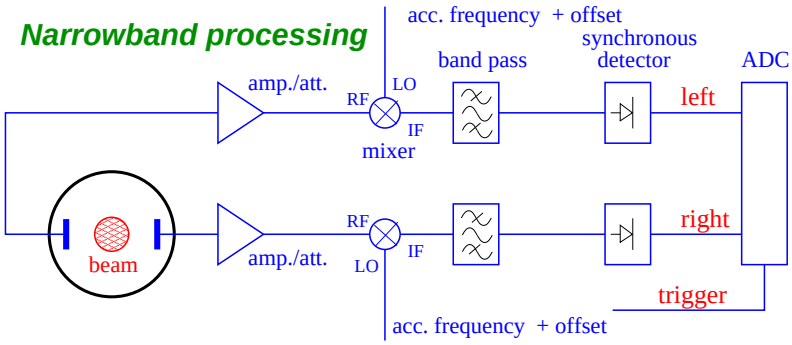

Fig. 41: Scheme of an analog narrowband processing.

For beams of non-relativistic velocities stored in a proton synchrotron this method can also be applied because the varying acceleration frequency is changed in phase with the bunch signal, resulting in a constant intermediate frequency at the IF-port [63].

This method is used for cavity BPMs to extract the amplitude of the resonating modes, which have a narrowband characteristics anyway. Here a significant noise reduction and mode separation is of importance due to the low signal strength.

To increase the accuracy a compensation of systematic errors can be performed by multiplexing the signals from the four BPM plates to a single channel chain, the scheme of such a system is depicted in Fig. 42. The main uncertainty arises from the gain- and offset-drifts of the amplifiers. However, if all four plate signals pass one single analog processing chain these drifts are compensated and do not effect the position accuracy for the difference-over-sum algorithm. The switching of the individual channels occurs at typically 10 kHz, which is much faster than typical time constants for the thermal drifts. The accuracy can further be improved by keeping the sum signal ΔU constant, which is performed by an automatic gain control loop acting on the pre-amplifier and IF amplifier gain. The general functionality is similar to the scheme without multiplexing: The single plate signal is mixed with a signal locked to the acceleration frequency including a certain offset. After bandpass filtering, the signal is rectified by a synchronous detector. For the quasi-dc signals the initial multiplexing is compensated in an analog manner to have individual plate outputs. These values are stored with the help of an analog sample&hold circuit and are provided for an external connection and digitalization after an active matrix; here a beam displacement proportional signal is generated by an analog manner as well. However, at a given instant of time, the signal from one plate is processed solely. This method can only be applied if any changes in

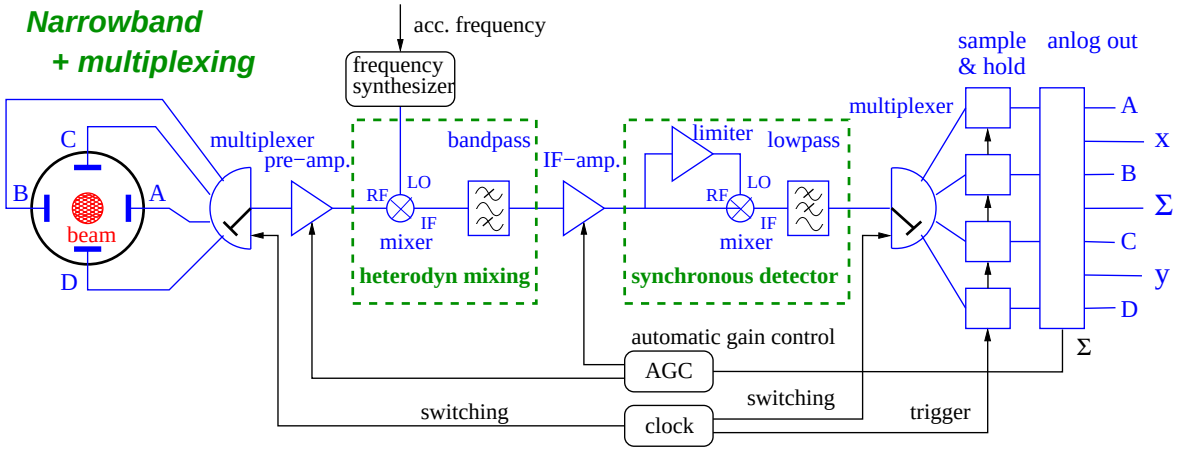

Fig. 42: Scheme of a narrowband processing with multiplexing.

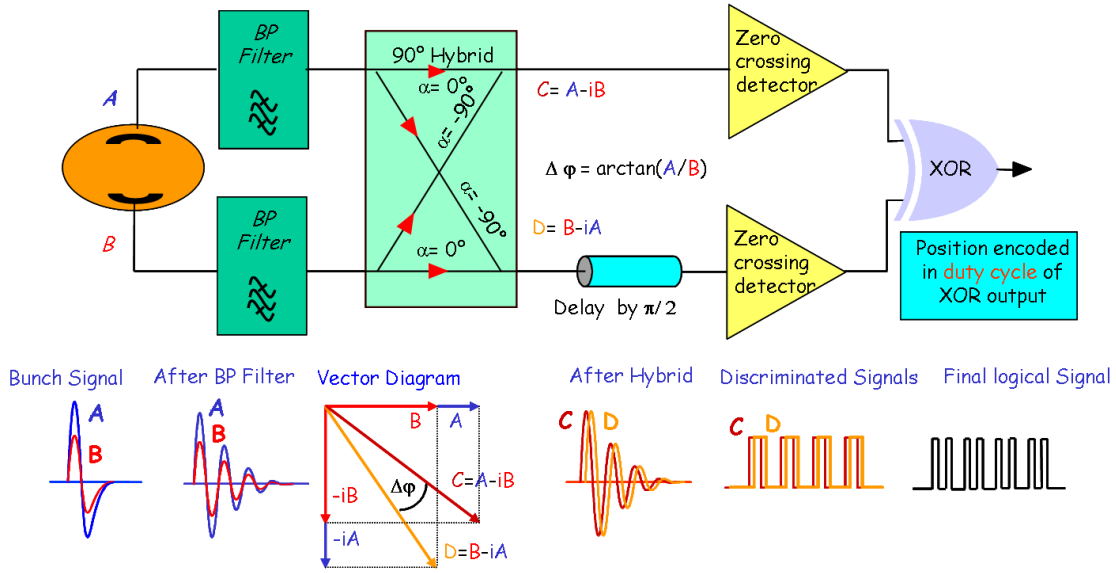

Fig. 43: Scheme of Amplitude-to-Phase Conversion AM/PM, from [54].

the beam parameters are much slower than the switching period of about 0.1 ms , which leads to severe restrictions for the usage of such a scheme. This popular analog electronics is commercially available [60].

The advantage of the narrowband processing is the very high resolution even for low beam currents due to a bandwidth restriction to a region of high signal amplitude. Additionally, this narrow bandwidth results in an effective noise reduction. However, by the narrow bandwidth any reference to the individual bunches or turns is lost. The choice of the IF-frequency and the lowpass filter characteristic determine the time resolution of such a system and the output bandwidth is at least a factor of thousand below the acceleration frequency. By multiplexing the four input signals to a single analog processing channel, systematic errors can be ruled out in an effective manner. The system is well suited for precise closed orbit measurements, but any beam parameter must be stable for a time of at least 10 ms.

7.5 Amplitude-to-Phase Conversion AM/PM

An analog method to transform the BPM plate voltages into logical signals is the Amplitude-to-Phase Conversion AM/PM. Such analog electronics can be installed close to the BPMs and the resulting logical pulses, which are less sensitive to any electro-magnetic interference, are transmitted via long cables out of the accelerator tunnel. The digitalization of logical pulses is straightforward and more cost-efficient compared to digitalization of voltages. The scheme of an AM/PM Conversion is shown in Fig. 43: The BPM signals *A* and *B* are bandpass filtered to generate a single working frequency for the electronic circuit. Each signal is split by a passive hybrid where one branch is used directly, while the other branch is shifted by -90^o (based on the processing bandpass-filter frequency) and added to the remaining signal from the opposite plate. As it can be seen from the vector representation, the resulting signals *C* and *D* have a phase shift, which depends on the amplitude ratio of the opposite BPM plates *A* and *B*. At this stage the amplitude is transformed to a phase shift what justifies the name AM/PM Conversion. With a phase detector the signals can be compared. Another possibility, as shown in the figure, is to detect the zero-crossing in an analog manner and to generate a logical pulse; one signal branch has to be delayed to arrive later than the signal from the other branch (independent of the plate's amplitude ratio). With the help of an Or-Gate the position can be transformed to a duty factor of logical pulses. For an AM/PM

Conversion the position reading is related to the BPM plate voltages by

$$x = \frac{1}{S_x} \cdot \left[\arctan\left(\frac{U_A}{U_B}\right) - 90^o \right] \tag{31}$$

with the position sensitivity now measured in $S_x = [\text{degree}/\text{mm}]$. Realizations of AM/PM Conversions are described e.g. in [64, 65, 66]. The scheme can be modified to achieve larger bandwidth (i.e. less sensitivity due to working frequency variations) by replacing the hybrid by a time delay and a combiner. The position information is then transformed into a length of a logical pulse; this is called wideband Amplitude-to-Time normalizer and is described in [67, 68, 69].

The advantage of AM/PM Conversion is the large dynamic range of up to ~ 60 dB without using a switchable gain amplifier. Within a dedicated analog circuit the plate voltages are converted to logical signals, which can be transferred by low-cost cables for straightforward digitalization. This method is well suited for large accelerators with many BPM locations. The disadvantage is the relatively complex analog electronics dedicated to only one frequency and the fact that a beam current proportional signal is not available. The bunches have to be well separated, to prevent any overlap of the filtered signal by successive bunches as required for the zero-crossing discriminator. The method does not work well for $f_{acc} > 150$ MHz. If one wants to use it for this frequency range an additional down conversion via heterodyn mixing is required, making these electronics even more complex.

7.6 Digital signal processing

The methods discussed above perform the BPM signal conditioning in an analog manner; for most cases it leads to a low bandwidth output, which is then digitized with a slow sampling ADC. Motivated by the intensive use in telecommunication, the properties of ADCs in terms of sampling rate and voltage resolution were significantly improved during the last decade. Additionally, the digital signal processing capabilities were enhanced. The tendency of modern technologies is to digitize the signal on an early stage of the signal path and replace the analog conditioning by digital signal processing. In most cases the required parallel processing is realized on an FPGA basis (Field Programmable Gate Array) to ensure fast, real-time response [70, 71]. On this digital basis, versatile treatments can be implemented without any hardware exchange. An example is the filtering of one data set with different bandwidths to match the position and time resolution to the requirements. The action of such a digital filter variation performed within one hardware board is depicted in Fig. 38.

The scheme of a commercially available electronics board [72, 73] designed for the usage at synchrotron light sources is shown in Fig. 44. Its general functionality is described in the following:

- The analog signal from the BPM plates (called A to D in the figure) are fed to a crossbar switch, where multiplexing is performed. In contrast to the switching for the analog narrowband case, each signal goes to one analog channel and all 4 BPM signals can be processed in parallel. The multiplexing is performed at an adjustable rate of typically 13 kHz.
- The analog signal is conditioned by a linear amplifier with switchable gain adjustments of 1 dB steps and a dynamic of about 30 dB to ensure a constant input level to the ADC. The gain setting to achieve constant output power is controlled using the amplitude value available in the digital part; the response time of about 10 s compensates slow thermal drifts.
- Analog bandpass filtering is performed with a relatively small bandwidth of about 10 MHz at the acceleration frequency of typically 352 or 500 MHz as used at most synchrotron light sources.
- The analog signal, conditioned in the described manner, is digitized with a fast, high resolution ADC having a maximum sampling rate of about 130 MS/s and a nominal resolution of 16 bit. The sampling frequency f_{sample} is locked to the acceleration frequency f_{acc} using the principle of under-sampling [74], as schematically depicted in Fig. 45: Due to the fact, that a sine wave can be reconstructed from 4 values, a periodicity of the digitized values is achieved if the sampling

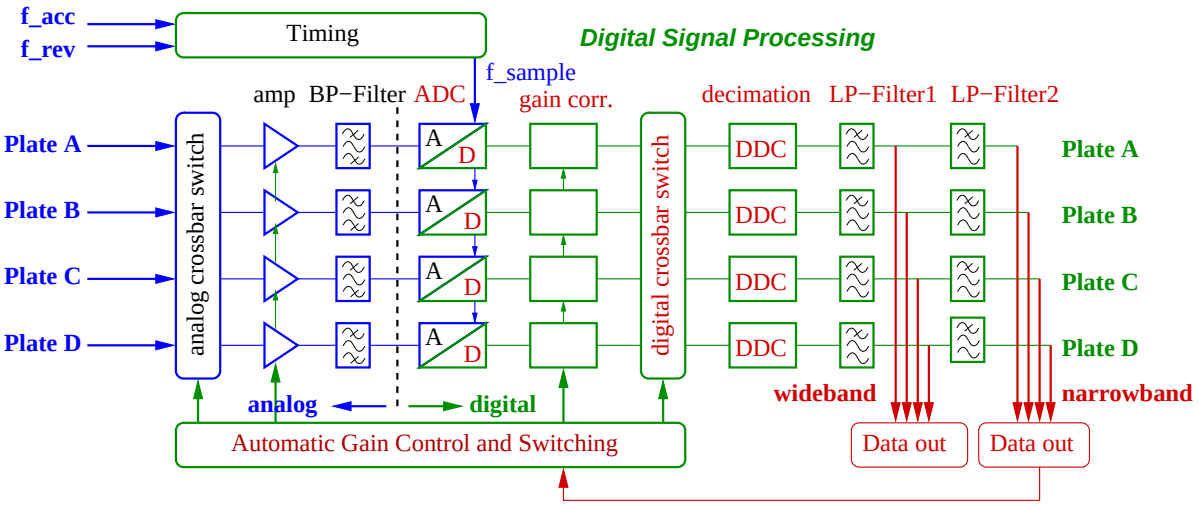

Fig. 44: Scheme of digital BPM electronics as typically used at the storage rings of synchrotron light sources.

frequency fulfills the condition $f_{sample} = \frac{4}{4n+1} \cdot f_{acc}$ with $n = 1, 2, 3....$ The value of n is chosen in such a way, that f_{sample} has the closest value below the maximal sampling rate of the ADC. In time-domain one can describe under-sampling in a way that a periodic signal is reconstructed from 4 digital values equally spaced over $4n+1$ periods. The resulting reconstructed sine-wave is called IF signal for intermediate frequency, according to its analog counterpart. For the typical case of a synchrotron light source with an acceleration frequency of $f_{acc} = 500$ MHz, the ADC is sampled at $f_{sample} = \frac{4}{4 \cdot 4+1} \cdot f_{acc} = 117.6$ MHz corresponding to $n = 4$. This means that the signal is mirrored to a band from zero to $f_{acc} - 4 f_{sample} = 32$ MHz. In time domain this case can be described such that 4 ADC values are equally distributed over 17 bunches.

- In the following block the digital data are corrected to compensate the analog multiplexing i.e. a correction related to the gain value of the input amplifier for the actual path is applied in a digital manner.
- The digital crossbar switch shifts the multiplexed signals back with respect to their original ordering.
- Now the data are demodulated by a Digital Down Converter DDC to a slightly lower frequency range resulting in a data reduction. The DDC is the corresponding digital device to the analog mixer [74].
- A digital filter increases the accuracy of the data. They are provided for external readout at the so called wideband port with a bandwidth of typically 10 kHz. The difference over sum algorithm is performed digitally using the data from this port.
- Further filtering, required for precise closed-orbit determination at a rate of typically 10 Hz is performed and the result is provided at the narrowband port. These digital values have the same usage and accuracy as generated in an analog manner by the multiplexed narrowband processing [75]. Moreover, the gain settings of the analog input amplifiers are controlled by these numerical values.

Due to the digital realization of the filter functions, the parameters can be adapted to the requirements by FPGA programming. The digital data can be used for monitoring and for a feedback system, simultaneously. If a turn-by-turn measurement is demanded, a single bunch is chosen as derived from the revolution frequency f_{rev} of typically 1 MHz to trigger the ADC.

At a proton synchrotron the acceleration frequency is lower than the maximum sample rate of the ADC and a direct sampling of the bunch signal after broadband amplification can be applied. With the

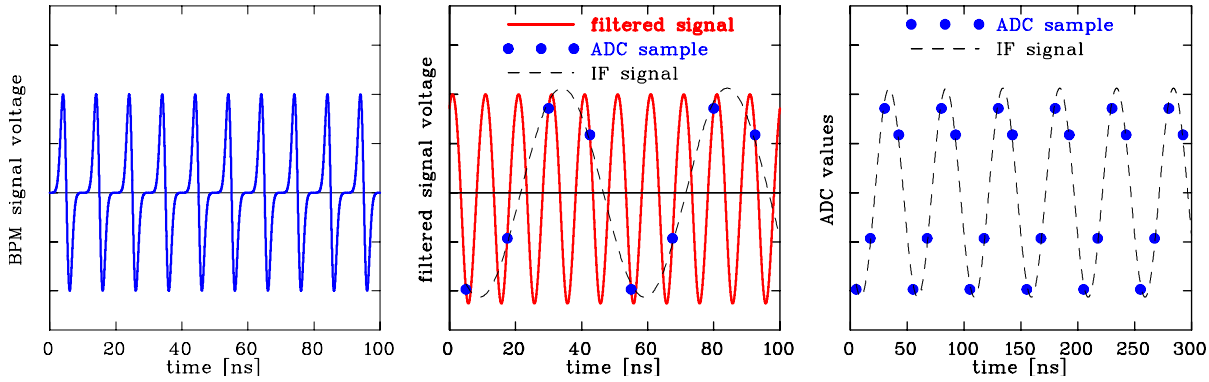

Fig. 45: The scheme shows the principle of under-sampling as performed for a BPM signal (left) filtered at the acceleration frequency (middle). The right plot shows the resulting digital values on an enlarged time scale. For this example the acceleration frequency is chosen as $f_{acc} = 100$ MHz and the sampling frequency is $f_{sample} = 4/5 \cdot f_{acc} = 80$ MHz, corresponding to four samples distributed over five bunches. The periodicity of the digital date is 50 ns corresponding to a bandwidth of 20 MHz for the reconstructed IF signal.

help of digital signal processing, the position of each bunch can be calculated resulting in a very flexible data acquisition system; an example is described in [56].

The advantage of digital signal processing is the great variability without hardware modification. Using digital filters, the bandwidth, data rate and therefore the position resolution can be varied over a wide range. Even the original data processed with different filters are digitally available and can be used for feedback purposes of different reaction times. For the digital processing a high resolution ADC with 14 bit is desirable, which limits the sampling rate to about 200 MS/s. For an acceleration frequency above this value under-sampling has to be applied, which results in some limitations for single bunch evaluations. There is no significant disadvantage of such systems. However, the versatile usage requires a large amount of engineering power for the FPGA programming as well as matched data exchange and analysis.

7.7 Comparison of BPM electronics

In Table 3 the advantages and disadvantages for the usual implementation of the discussed electronics schemes are summarized. Electronics can be adapted to the requirements in a flexible manner to partly compensate the related disadvantages. The applicability of various schemes is mainly fixed by the necessary performance and the financial investments required for the manifold BPM locations.

For a pure analog signal processing scheme, the logarithmic ratio has the advantage being very robust as well as cost efficient and is therefore suited for industrial applications, where a low accuracy might be acceptable. Analog narrowband processing gives a high accuracy, but cannot be adapted to the requirements in a flexible manner. Digital signal processing delivers nearly the same accuracy. The flexibility without hardware exchange is the key advantage for this modern scheme, which opens the possibility of versatile usage of position data. At nearly all new accelerators the BPM readout is realized in such a way. For a proton synchrotron with an acceleration frequency $f_{acc} \leq 10$ MHz, the BPM signal is amplified on a broadband basis preserving the bunch structure and the sampling is even performed in the baseband; the position is than calculated by digital signal processing.

8 Summary

BPMs serve as a versatile non-destructive device for the determination of the beam's center-of-mass. The signal strength and shape can be calculated using the transfer impedance Z_t. The signal properties can widely be influenced by the choice of the impedance coupling and pre-amplifier properties. Several BPM

Table 3: Simplified comparison between various electronic processing schemes

Type	Usage	Precaution	Advantage	Disadvantage
Broadband	p-acc	f_{acc} < 300MHz	bunch structure monitoring post processing possible required for fast feedback	resolution limited by noise extensive hardware
Log-ratio	all	bunch train $\geq 1\mu$s	robust electronics very high dynamic range cheap and easy usage	limited bunch resolution large thermal drift limited accuracy
Narrowband	all	stable beams $\geq 10\mu$s	high resolution low detection threshold	no turn-by-turn complex electronics
Narrowband + multiplexing	all	stable beams ≥ 10ms	highest resolution low detection threshold high accuracy	no turn-by-turn complex electronics only for stable storage
AM/PM	all	limited f_{acc} low bunching	only two channels high dynamics range	special analog circuits no intensity signal only for constant f_{acc}
Digital Signal Processing	all	some bunches ADC with $\simeq 200$MS/s	very flexible high resolution modern technology for future demands	limited time resolution due to under-sampling extensive hardware complex technology

types matched to typical applications were described: The linear-cut type is used at a proton synchrotron operating with low acceleration frequencies. This type offers a very linear position sensitivity but the mechanical realization is quite extensive. The mechanics for the button type is simpler, but non-linearities for the position reading occur. This type is used at proton and electron accelerators within various configurations. For short bunches the signal propagation along the BPM has to be considered and stripline BPMs are used if a signal deformation must be avoided. Moreover, with this type one can distinguish counter-propagating beams. But strong mechanical requirements have to be fulfilled, in particular related to the 50 Ω matching at the ports. Cavity BPMs are recently realized due to the requirement of precise position determination for short beam pulses.

Quite different electronic principles are commonly used. As given by the thermal noise contribution, one can chose between high position resolution at longer 'averaging' time, or lower position resolution at a faster data refresh i.e. the position resolution and the time resolution are counteracting quantities. The different requirements lead to various schemes, which are traditionally realized in an analog manner. Broadband and narrowband analog processing define the two extreme cases concerning position and time resolution. The tendency at modern facilities is to digitize the signal at an early stage and use digital signal processing for the necessary signal conditioning. However, the digitalization by state-of-the-art ADCs with about 200 MS/s gives some restrictions for the applicability of digital signal processing.

Acknowledgment: The careful proof-reading by Ute Meier is gratefully acknowledged.

References

[1] R.E. Shafer, *Proc. Beam Instr. Workshop BIW 89*, Upton, p. 26, available e.g. at www.bergoz.com/products/MX-BPM/MX-BPM-downloads/files/Shafer-BPM.pdf (1989).

[2] S.R. Smith, *Proc. Beam Instr. Workshop BIW 96*, Argonne AIP 390, p. 50 (1996).

[3] G.R. Lambertson, *Electromagnetic Detectors*, Proc. Anacapri, Lecture Notes in Physics 343,

Springer-Verlag, p. 380 (1988).

[4] E. Schulte, in *Beam Instrumentation*, CERN-PE-ED 001-92, revised Nov. 1994 p. 129 (1994).

[5] D.P. McGinnis, *Proc. Beam Instr. Workshop BIW 94,* Vancouver, p. 64 (1994).

[6] J.M. Byrd, Bunched Beam Signals in the time and frequency domain, in *Proceeding of the School on Beam Measurement*, Montreux, p. 233 World Scientific Singapore (1999).

[7] J. Hinkson, ALS Beam Instrumentation, available e.g. at www.bergoz.com/products/MX-BPM/MX-BPM-downloads/files/Hinkson-BPM.pdf (2000).

[8] W. Kaufmann, J. Schölles, *Proc. DIPAC 03*, Mainz, p 208 (2003).

[9] Textbooks on Digital Signal Processing, e.g. U. Tietze, Ch. Schenk, E. Gamm, *Electronic Circuits*, Springer Verlag (2008).

[10] M. Hoffmann, in *Proc. CAS on Digital Signal Processing*, Sigtuna, CERN 2008-003, p. 11 (2008).

[11] G. Kube, M. Werner, *Proc. DIPAC 05*, Venice, (2007).

[12] P. Kowina et al., *Proc. DIPAC 05*,, Lyon, p. 114 (2005)

[13] P. Kowina, *CARE-ABI Workshop Lüneburg 2006,* see adweb.desy.de/mdi/CARE/Lueneburg/ABI-Lueneburg.htm (2006) and P. Kowina et al., *Proc. EPAC 06,* Edinburgh, p. 1022 (2006).

[14] P. Kowina et al., *Proc. DIPAC 07*, Venice (2007).

[15] J.H. Cuperus, *Nucl. Instrum. Meth.* **145**, p. 233 (1977).

[16] B.G. Pine, *CARE-ABI Workshop Lüneburg 2006,* see adweb.desy.de/mdi/CARE/Lueneburg/ABI-Lueneburg.htm (2006).

[17] B. G. Pine et al., *Proc. EPAC 06*, Edinburgh, p. 1082 (2006).

[18] C. Boccard, *CARE-ABI Workshop Lüneburg 2006,* see adweb.desy.de/mdi/CARE/Lueneburg/ABI-Lueneburg.htm (2006).

[19] R.E. Shafer, *Proc. Beam Instr. Workshop BIW 1993,* Santa Fe, p. 303 (1994).

[20] S.J. Park et al., *Proc. DIPAC 03*, Mainz, p 199 (2003).

[21] P. Kowina et al., in preparation for *Proc. DIPAC 09*, Basel (2009).

[22] N. Kurita et al., *Proc. PAC 95,* Dallas, p. 2512 (1995), C.K. Ng et al, *Proc. PAC 95*, Dallas, p. 2485 (1995).

[23] T. Shintake et al. Nucl. Instrum. Meth. **A 254**, 146 (1987).

[24] S. Varnasseri et al., *Proc. DIPAC 05*, Lyon, p. 90 (2005).

[25] Textbooks for Microwave Engineering, e.g. D.M. Pozar, *Microwave Engineering*, John Wiley, New York (1998).

[26] D. Nölle, M. Wendt, *Proc. LINAC 04*, Lübeck, p. 435 (2004).

[27] D. Nölle et al., *Proc. LINAC 04*, Lübeck, p. 426 (2004).

[28] T.J. Shea, R.L. Witkover, *Proc. Beam Instr. Workshop BIW 98,* Stanford AIP 451, p. 145 (1998).

[29] M. Bai et al., Nucl. Instrum. Meth. **A 499**, 372 (2003).

[30] S.S. Kurennoy, R.E. Shafer, *Proc. EPAC 2000,* Vienna p. 1765 and p. 1768 (2000).

[31] S.S. Kurennoy, *Proc. PAC 07,* Albuquerque, p. 4111 (2007) and J.F. O'Hara et al., *Proc. PAC 07*, Albuquerque, p. 4123 (2007).

[32] L. Sørby, *CARE-ABI Workshop Lüneburg 2006,* see adweb.desy.de/mdi/CARE/Lueneburg/ABI-Lueneburg.htm (2006).

[33] S. Battisti et al., *Proc. PAC 87*, Washington, p. 605 (1987).

[34] A. Chapman-Hatchett, A. Jansson, D.J. William, *Proc. PAC 99*, New York, p. 2223 (1999) and A. Jansson, D.J. William, *Nucl. Instr. Meth.*, **A 479**, p. 233 (2002).

[35] V.A. Verzilov et al., *Proc. CYCLOTRONS 07*, Giardini Nexos, p.331 (2007).

[36] D. McGinnis, *Proc. PAC 99*, New York, p. 1713 (1999).

[37] F. Nolden et al., *Proc. PAC 05*, Knoxville, p. 799 (2005).

[38] F. Caspers et al., *Proc. PAC 07*, Albuquerque, p. 4174 (2007).

[39] S. Hancock, M. Lindroos, S. Koscielniak, *Phys. Rev. Special Topic Acc. Beam*, **3**, 124202 (2000) and CERN-PS-2000-068-OP (2000).

[40] B. Fellenz, J. Crisp, *Proc. Beam Instrum. Workshop BIW 98*, Stanford, p. 446 (1998).

[41] P. Odier, *Proc. DIPAC 03*, Mainz, p. 218 (2003).

[42] e.g. T. Lefevre et al., *Proc. Beam Instrum. Workshop BIW 08*, Lake Tahoe (2008).

[43] R. Webber, *Proc. Beam Instrum. Workshop BIW 89*, Upton, p. 85 (1989).

[44] M. Gasior, *Proc. DIPAC 05*, Lyon, p. 175 (2005) and M. Gasior, *Proc. DIPAC 03*, Mainz, p. 53 (2003).

[45] R. Lorenz, *Proc. Beam Instr. Workshop BIW 98*, Stanford AIP 451, p. 53 (1998).

[46] Textbook on microwave engineering or electro-dynamics, e.g. J.D. Jackson, *Classical Electrodynamics*, John Wiley & Sons (1998).

[47] T. Weiland et al., *Proc. CAS on Radio Frequency Engineering*, Seeheim, CERN 2005-003 (2004).

[48] A. Lunin et al., *Proc. DIPAC 07*, Venice, (2007).

[49] M. Wendt, *CARE-ABI Workshop Lüneburg 2006*, see adweb.desy.de/mdi/CARE/Lueneburg/ABI-Lueneburg.htm (2006).

[50] S. Walston et al., *Nucl. Instrum. Meth.* A 678, p. 1 (2007).

[51] C. Simon et al., Phys. Rev. Acc. and Beams, 11, 082802 (2008).

[52] V. Schlott et al., *Proc. DIPAC 01*, Grenoble, p. 69 (2001) and M. Dehler et al, *Proc. PAC 99*, New York, p. 2087 (1999).

[53] P. Pollet, T. Schilcher, *CARE-ABI Workshop Hamburg 2004*, see adweb.desy.de/mdi/Conferencesold/Aumuehle/CARE-N3-Aumuehle-Agenda.html (2004).

[54] G. Vismara, *Proc. Beam Instr. Workshop BIW 2000*, Cambridge AIP 546, p. 36 (2000) and G. Vismara, *Proc. DIPAC 99*, Chester, p. 11 (1999).

[55] J. Schölles, W. Kaufmann, *Proc. DIPAC 05*, Lyon, p. 190 (2005).

[56] J. Belleman, *Proc. DIPAC 05*, Lyon, p. 137 (2005) and J. Belleman et al., *Proc. DIPAC 07*, Venice (2007).

[57] F.D. Wells et al., *Proc. PAC 91*, San Francisco, p. 1139 (1991) and F.D. Wells et al., *Proc. PAC 93*, Washington, p. 2316 (1993).

[58] R.E. Shafer, *Proc. Beam Instr. Workshop BIW 92*, Berkeley, p.120 (1992) and G.R. Aiello, M.R. Mills, *Proc. Beam Instr. Workshop BIW 92*, Berkeley, p. 301 (1992).

[59] H. Schmickler, G. Vismara, *Proc. DIPAC 01*, Grenoble, p. 186 (2001).

[60] Company Bergoz Instrumentation, www.bergoz.com.

[61] R. Biscardi, J.W. Bittner, *Proc. PAC 89*, Chicago, p. 1516 (1989).

[62] J. Hinkson, K. Unser, *Proc. DIPAC 95*, Travemünde, p. 124 (1995) and K. Unser, *Proc. Beam Instr. Workshop BIW 96*, Argonne, p. 527 (1996) available at www.bergoz.com/products/MX-BPM/MX-BPM-downloads/downloads.html.

[63] P. Moritz *Proc. DIPAC 95*, Travemünde, p. 121 (1995) and P. Moritz, K. Beckert, *Proc. DIPAC 93*, Montreux (1993).

[64] S.P. Jachim, R.C. Webber, R.E. Shafer, *Proc. PAC 81*, Washington, p. 2323(1981).

[65] G. Vismara, *Proc. EPAC 94*, London, p. 1458 (1994).

[66] M. Wendt, *Proc. DIPAC 01*, p. 63 (2001).

[67] D. Cocq, *Nuncl. Instrum. Meth.* **A 416**, p. 1 (1998).

[68] E. Calvo et al., *Proc. DIPAC 03*, Mainz, p. 187 (2003).

[69] R. Jones, *Proc. PAC 07,* Albuquerque, p. 2630 (2007).

[70] e.g. J. Serano, in *Proc. CAS on Digital Signal Processing*, Sigtuna, CERN 2008-003, p. 231 (2008).

[71] e.g. M. Dehler, in *Proc. CAS on Digital Signal Processing*, Sigtuna, CERN 2008-003, p. 331 (2008).

[72] Company Instrumentation Technology, www.i-tech.si.

[73] A. Kosicek, *Porc. PAC 05*, Knoxville p. 4284 (2005) and R. Ursic, *Proc. PAC 99*, New York, p. 2253 (1999).

[74] e.g. T. Schilcher, in *Proc. CAS on Digital Signal Processing*, Sigtuna, CERN 2008-003, p. 249 (2008).

[75] P. Hartmann et al., *Proc. DIPAC 07,* Venice, (2007).